OPTIMUM DESIGN OF CERAMIC TENSILE CREEP SPECIMEN USING FINITE ELEMENT METHOD

A thesis submitted in partial fulfillment of
the requirements for the award of degree
of

MASTER OF ENGINEERING
in
CAD/CAM & ROBOTICS

BY

SAURABH KHERA
Roll No - 80681019

under the guidance of

Mr. J. S. SAINI
Lecturer
Mechanical Engineering Department

Mechanical Engineering Department
THAPAR UNIVERSITY, PATIALA-147004
June 2008

CERTIFICATE

I hereby certify that the work which is being presented in the thesis entitled, ***"OPTIMUM DESIN OF CERAMIC TENSILE CREEP SPECIMEN USING FINITE ELEMENT METHOD"***, in partial fulfillment of the requirements for the award of degree of ***MASTER OF ENGINEERING IN MECHANICAL ENGINEERING*** submitted in ***MECHANICAL ENGINEERING DEPARTMENT OF THAPAR UNIVERSITY, PATIALA*** is an authentic record of my own work carried out under the supervision of ***Mr. J.S. SAINI*** and refers other researcher's works which are duly listed in the reference section.

The matter presented in this thesis has not been submitted for the award of any other degree of this or any other university.

Saurabh

(SAURABH KHERA)

This is to certify that the above statement made by the candidate is correct and true to the best of my knowledge.

(Mr. J.S. SAINI) 30/6/08
Lecturer, MED

Countersigned by

10/7/08

(Dr. S.K. MOHAPATRA)
Professor & Head, MED
Thapar University, Patiala

(Dr. R.K. SHARMA)
Dean Academic Affairs
Thapar University, Patiala

ACKNOWLEDGEMENT

Words are often less to revels one's deep regards. With an understanding that work like this can never be the outcome of a single person, I take this opportunity to express my profound sense of gratitude and respect to all those who helped me through the duration of this work.

This work would not have been possible without the encouragement and able guidance of my supervisor ***Mr. J.S. SAINI***. His enthusiasm and optimism made this experience both rewarding and enjoyable. Most of the novel ideas and solutions in this work are the result of our numerous stimulating discussions. His feedback and editorial comments were also invaluable for the writing of this thesis. I am grateful to ***Dr. S.K. MOHAPATRA***, Prof. & Head, MED for providing the facilities for the completion of the work.

I take pride of myself being son of ideal parents for their everlasting desire, sacrifice, affectionate blessings and help, without which it would not have been possible for me to complete my studies.

At last, I would like to thank to all the members and employees of Mechanical Engineering Department, Thapar University, Patiala for their everlasting support.

Regards,

(*SAURABH KHERA*)

ABSTRACT

An optimization procedure for designing a ceramic tensile creep specimen to minimize stress concentration is carried out using finite element method. The effect of pin loading and the specimen geometry are considered in the stress distribution calculations. A growing contact zone between the pin and the specimen has been incorporated into the problem solution scheme as the load is increased to its full value. The optimization procedures are performed for the specimen, and all design variables including pinhole location and pinhole diameter, head width, neck radius, and gauge length are determined based on a set of constraints imposed on the problem. In addition, for the purpose of assessing the possibility of delayed failure outside the gage section, power-law creep in the tensile specimen is considered in the analysis. Using a particular grade of advanced ceramics as an example, it is found that if the specimen is not designed properly, significant creep deformation and stress redistribution may occur in the head of the specimen resulting in undesirable (delayed) head failure of the specimen during the creep test.

TABLE OF CONTENTS

CERTIFICATE			**i**
ACKNOWLEDGEMENT			**ii**
ABSTRACT			**iii**
TABLE OF CONTENTS			**iv-v**
LIST OF FIGURES			**vi-viii**
LIAT OF TABLES			**ix**
CHAPTER 1	**INTRODUCTION**		**1-5**
	1.1	CERAMICS	1-2
	1.2	APPLICATION AREAS OF CERAMICS	2-3
	1.3	CREEP	3-5
CHAPTER 2	**LITERATURE REVIEW**		**6-15**
	2.1	LITERATURE REVIEW	6-15
CHAPTER 3	**FEM FORMULATION**		**16-28**
	3.1	BASIC FINITE ELEMENT PROCEDURE	16-19
	3.2	MATHEMATICAL MODEL FOR CREEP	19-21
	3.3	PLANE STRESS ANALYSIS	22-25
	3.4	PLANE STRAIN ANALYSIS	25-27
	3.5	TIME INCREMENT SELECTION	27-28
CHAPTER 4	**RESULS AND DISCUSSIONS**		**29-57**
	4.1	ELASTIC STRESSES IN THE SPECIMEN	31-34
	4.2	VALIDATION	35-39
	4.3	ALLOWABLE STRESSES	40
	4.4	ELASTIC STRESSES IN OPTIMUM DESIGN	41
	4.5	CREEP BEHAVIOR	42-47
	4.6	VALIDATION OF CREEP RESULTS	48-57
CHAPTER 5	**CONCLUSION AND SCOPE FOR FUTURE WORK**		**58**
	5.1	CONCLUSION	58

5.2 SCOPE FOR FUTURE WORK 58

REFERENCES **59-61**

BIBLIOGRAPHY **62-64**

LIST OF FIGURES

Fig 1.1 Creep Behavior 5

Fig 3.1 Basic Stiffness Element for Plane Stress Analysis 22

Fig 4.1 Initial design of the tensile creep specimen 29

Fig. 4.2(a) Hole stress of the specimen as a function of head width W 31

Fig. 4.2(b) Hole stress of the specimen as a function of hole location L1 32

Fig. 4.2(c) Hole stress of the specimen as a function of gage length GL 32

Fig. 4.2(d) Hole stress of the specimen as a function of neck radius R 33

Fig. 4.3(a) Head stress of the specimen as a function of hole location L1 33

Fig. 4.3(b) Head stress of the specimen as a function of head width W 34

Fig. 4.4 Neck stress of the specimen as a function of neck radius R 34

Fig 4.5 Initial specimen (Meshed) 35

Fig 4.6 Equivalent Stress Distribution from the Contact Analysis (Including Pins) 35

Fig 4.7 Equivalent Stress Distribution from the Contact Analysis (Excluding Pins) 36

Fig. 4.8 Comparison of hole stress as a function of neck radius R (ANSYS vs program) 36

Fig. 4.9 Comparison of hole stress as a function of gauge length GL (ANSYS vs program) 37

Fig. 4.10 Comparison of hole stress as a function of hole location L1 (ANSYS vs program) 37

Fig. 4.11 Comparison of hole stress as a function of neck radius R (ANSYS vs program) 38

Fig. 4.12 Comparison of head stress as a function of hole location L1 (ANSYS vs program) 38

Fig. 4.13 Comparison of head stress as a function of head width W (ANSYS vs program) 39

Fig. 4.14 Comparison of neck stress as a function of neck radius R (ANSYS vs program) 39

Fig 4.15 Optimum Designed Specimen 40

Fig 4.16 Equivalent stress distribution in optimum design from contact analysis 41
(including pins)
Fig 4.17 Equivalent stress distribution in optimum design from contact analysis 41
(excluding pins)
Fig 4.18 Creep stress redistribution: Equivalent stress at t=1 42
Fig 4.19 Creep stress redistribution: Equivalent stress at t=50 42
Fig 4.20 Creep stress redistribution: Equivalent stress at t=100 43
Fig 4.21 Creep stress redistribution: Equivalent stress at t=1 43
Fig 4.22 Creep stress redistribution: Equivalent stress at t=50 44
Fig 4.23 Creep stress redistribution: Equivalent stress at t=100 44
Fig. 4.24 Creep stresses experienced at various critical points as a function of time for initial specimen design ***45***
Fig. 4.25 Creep stresses experienced at various critical points as a function of time for final specimen design ***46***
Fig. 4.26 Creep strains experienced at the corresponding locations for initial specimen design 47
Fig. 4.27 Creep strains experienced at the corresponding locations for final specimen design 47
Fig. 4.28 Comparison of creep stress at head section 48
(ANSYS vs Program: For Initial Specimen)
Fig. 4.29 Comparison of creep stress at load section 48
(ANSYS vs Program: For Initial Specimen)
Fig. 4.30 Comparison of creep stress at hole section 49
(ANSYS vs Program: For Initial Specimen)
Fig. 4.31 Comparison of creep stress at neck section 49
(ANSYS vs Program: For Initial Specimen)
Fig. 4.32 Comparison of creep stress at gauge section 50
(ANSYS vs Program: For Initial Specimen)
Fig. 4.33 Comparison of creep stress at head section 50
(ANSYS vs Program: For Optimized Specimen)
Fig. 4.34 Comparison of creep stress at load section 51
(ANSYS vs Program: For Optimized Specimen)
Fig. 4.35 Comparison of creep stress at hole section 51
(ANSYS vs Program: For Optimized Specimen
Fig. 4.36 Comparison of creep stress at neck section 52

(ANSYS vs Program: For Optimized Specimen)
Fig. 4.37 Comparison of creep stress at gauge section 52
(ANSYS vs Program: For Optimized Specimen
Fig. 4.38 Comparison of equivalent creep strain at head section 53
(ANSYS vs Program: For Initial Specimen)
Fig. 4.39 Comparison of equivalent creep strain at load section 53
(ANSYS vs Program: For Initial Specimen)
Fig. 4.40 Comparison of equivalent creep strain at hole section 54
(ANSYS vs Program: For Initial Specimen)
Fig. 4.41 Comparison of equivalent creep strain at neck section 54
(ANSYS vs Program: For Initial Specimen)
Fig. 4.42 Comparison of equivalent creep strain at gauge section 55
(ANSYS vs Program: For Initial Specimen)
Fig. 4.43 Comparison of equivalent creep strain at head section 55
(ANSYS vs Program: For Optimized Specimen
Fig. 4.44 Comparison of equivalent creep strain at load section 56
(ANSYS vs Program: For Optimized Specimen)
Fig. 4.45 Comparison of equivalent creep strain at hole section 56
(ANSYS vs Program: For Optimized Specimen)
Fig. 4.46 Comparison of equivalent creep strain at neck section 57
(ANSYS vs Program: For Optimized Specimen)
Fig. 4.47 Comparison of equivalent creep strain at gauge section 57
(ANSYS vs Program: For Optimized Specimen)

LIST OF TABLES

Table 1.1 Applications of ceramics 3

CHAPTER 1
INTRODUCTION

1.1 CERAMICS

The word ceramic derives its name from the Greek ***keramos***, meaning "pottery", which in turn is derived from an older Sanskrit root, meaning "to burn". The Greeks used the term to mean "burnt stuff" or "burned earth". Thus the word was used to refer to a product obtained through the action of fire upon earthy materials.

Ceramics can be defined as inorganic, non-metallic materials that are typically produced using clays and other minerals from the earth or chemically processed powders. Ceramics are typically crystalline in nature and are compounds formed between metallic and non-metallic elements such as aluminium and oxygen (alumina- Al_2O_3), silicon and nitrogen (silicon nitride- Si_3N_4) and silicon and carbon (silicon carbide-SiC). Glass is often considered a subset of ceramics. Glass is somewhat different than ceramics in that it is amorphous, or has no long-range crystalline order.

1.1.1 CLASSIFICATION OF CERAMICS

Ceramics can be classified as:

- *Structural*, including bricks, pipes, floor and roof tiles
- *Refractories*, such as kiln linings, gas fire radiants, steel and glass making crucibles
- *Whitewares*, including tableware, wall tiles, decorative art objects and sanitary ware
- *Technical*, such items include tiles used in the space shuttle program, gas burner nozzles, ballistic protection, nuclear fuel uranium oxide pellets, bio-medical implants, jet engine turbine blades, and missile nose cones.

1.1.2 PROPERTIES OF CERAMICS

Ceramics have the following important inherent properties:

- Hard (wear resistant).
- Resistant to plastic deformation.
- Resistant to high temperatures.
- Good corrosion resistance.
- Low thermal conductivity.
- Low electrical conductivity.

However, some ceramics exhibit high thermal conductivity and/or high electrical conductivity. The combination of these properties means that ceramics can provide:

- High wear resistance with low density.
- Wear resistance in corrosive environments.
- Corrosion resistance at high temperatures.

1.2 APPLICATION AREAS OF CERAMICS

Ceramics offer many advantages compared to other materials. They are harder and stiffer than steel; more heat and corrosion resistant than metals or polymers; less dense than most metals and their alloys; and their raw materials are both plentiful and inexpensive. Because of their high temperature strength, oxidation and corrosion resistance, and superior wear performance, advanced ceramics (e.g., silicon nitride, silicon carbide, alumina, etc.) are promising materials for use in high temperature, load-bearing applications such as turbine engines, heat exchangers and waste incinerators. Ceramic materials display a wide range of properties, which facilitate their use in many different product areas. Various applications of ceramics are displayed in the Table 1.1 below:

PRODUCT AREA	APPLICATION
Aerospace	Space Shuttle Tiles, Thermal Barriers, High Temperature Glass Windows, Fuel Cells

Consumer Uses	Glassware, Windows, Pottery, Corning Ware, Magnets, Dinnerware, Ceramic Tiles, Lenses, Home Electronics, Microwave Transducers
Automotive	Catalytic Converters, Ceramic Filters, Airbag Sensors, Ceramic Rotors, Valves, Spark Plugs, Pressure Sensors, Thermistors, Vibration Sensors, Oxygen Sensors, Safety Glass Windshields, piston Rings
Medical (Bioceramics)	Orthopedic Joint Replacement, Prosthesis, Dental Restoration, Bone Implants
Military	Structural Components for Ground, Air and Naval Vehicles, Missiles, Sensors
Computers	Insulators, Resistors, Superconductors, Capacitors, Ferroelectric Components, Microelectronic Packaging
Other Industries	Bricks, Cement, Membranes and Filters, Lab Equipment
Communications	Fiber Optic/Laser Communications, TV and Radio Components, Microphones

Table 1.1: Applications of ceramics

1.3 CREEP

Creep is the term used to describe the tendency of a material to move or to deform permanently to relieve stresses. Material deformation occurs as a result of long-term exposure to levels of stress (physics) that are below the yield strength or ultimate strength of the material. Creep is more severe in materials that are subjected to heat for long periods and near melting point. Creep is a monotonically increasing function of temperature.

The rate of this deformation is a function of the material properties, exposure time, exposure temperature and the applied load (stress). Depending on the magnitude of the applied stress and its duration, the deformation may become so large that a component can no longer perform its function — for example creep of a turbine blade will cause the blade to contact the casing, resulting in the failure of the blade. Creep is usually of concern to engineers and metallurgists when evaluating components that operate under high stresses or high temperatures. Creep is not necessarily a failure mode, but is instead a deformation mechanism.

Unlike brittle fracture, creep deformation does not occur suddenly upon the application of stress. Instead, strain accumulates as a result of long-term stress. Creep deformation is "time-dependent" deformation.

The temperature range in which creep deformation may occur differs in various materials. For example, tungsten requires a temperature in the thousands of degrees before creep deformation can occur while ice formations such as the Antarctic ice cap will creep in freezing temperatures. Generally, the minimum temperature required for creep deformation to occur is 30-40% of the melting point for metals and 40-50% of melting point for ceramics. Virtually any material will creep upon approaching its melting temperature. Since the minimum temperature is relative to melting point, creep can be seen at relatively low temperatures for some materials.

1.3.1 CREEP BEHAVIOR

Experimental creep data (using constant stress and temperature) often display three different types of behavior for the creep strain rate as function of time.

- In the initial primary creep regime the creep strain rate is decreasing with time.
- In the secondary creep regime the creep strain rate is almost constant.
- In the final tertiary creep regime the creep strain rate is increasing with time until a failure occurs.

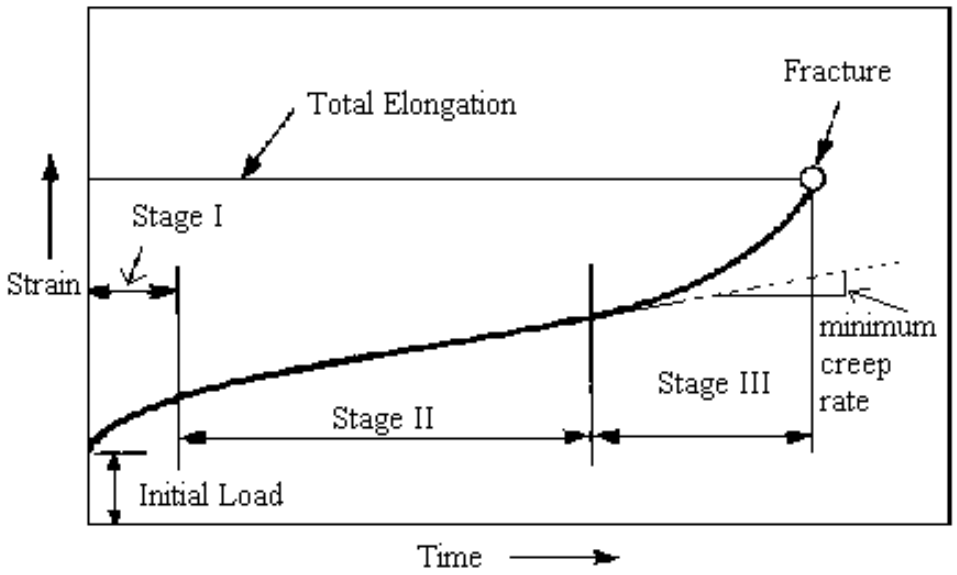

Fig 1.1: Creep Behavior

The part of the curve, which is of interest to designers, is the straight one. Steady state creep often takes up most of the time in a creep test. The knowledge of the creep rate allows to estimate how much time is needed until a component reaches a certain deformation and, for example, becomes incompatible with the geometry of the system it is part of. The jet engine is a good example. The gap between the tip of the rotating blades and the engine casing has to be very small in order to maximize the engine efficiency in that the amount of gas that flows through the engine without acting on the blades is kept as small as possible. However, if a blade elongates too much as a result of creep, it ends up scraping against the inner wall of the casing causing serious damage. Jet engine manufacturers and users don't want this to happen! If, however, the creep rate of the material is known along with the lifetime already spent by the blades, these can be replaced before the irreparable happens.

CHAPTER 2
LITERATURE REVIEW

The following section shows the work done by various researchers in the field of creep testing on ceramics.

2.1 LITERATURE REVIEW

Daniel f. Carroll et. al. [1] in 1988 studied accumulation of creep damage in a siliconized silicon carbide. The accumulation was investigated as a function of applied stress, creep strain, and microstructure. At 1100°C, creep damage was observed to accompany deformation in specimens tested to creep strains greater than 0.10%, under applied stresses greater than 137 MPa. At low creep strains, creep damage occurred in regions of the microstructure of high silicon carbide content. As deformation progressed, creep damage extended into regions of the microstructure of lower silicon carbide content. The area density and area fraction of cavities were found to increase linearly with creep strain. From these results, a threshold stress for the formation of creep damage was determined to be 132 MPa at 1100°C. It was suggested that the formation of creep damage was controlled by the heterogeneous nucleation of cavities at the silicon-silicon carbide interface, with the aid of high localized stresses and iron impurities in the silicon phase.

Sheldon M. Wiederhorn et. al. [2] in 1988 studied damage-enhanced creep in a siliconized silicon carbide. The creep behavior of a commercial grade of reaction-bonded silicon carbide was characterized at a temperature of 1300°C. Creep occurred more easily in tension than in compression. At a given applied stress, the steady-state creep rate in tension was found to be at least 20 times that obtained in compression. In both tension and compression, the stress exponent for steadystate creep was found to increase with increasing applied stresses. At low applied stresses, the stress exponent was 4, suggesting some kind of dislocation mechanism operating in the two-phase composite. At high stresses, the stress exponent was 11 in tension. The increase in the stress exponent was attributed to damage accumulation in the form of cavities. An effective threshold stress for cavitation of less than 100 MPa was suggested. In

compression, the cause of the increase of stress exponent with stress cannot be attributed to cavitation.

Daniel F. Carroll et. al. [3] in 1989 studied the effect of creep damage on the tensile creep behavior of a siliconized silicon carbide. The tensile creep behavior of a siliconized silicon carbide was investigated in air, under applied stresses of 103 to 172 MPa for the temperature range of 1100° to 1200°C. At 1100°C, the steady-state stress exponent for creep was approximately 4 under applied stresses less than the threshold for creep damage (132 MPa). At applied stresses greater than the threshold stress for creep damage, the stress exponent increased to approximately 10. The activation energy for steady-state creep at 103 MPa was approximately 175 kJ/mol for the temperature range of 1100° to 1200°C. Under applied stresses of 137 and 172 MPa, the activation energy for creep increased to 210 and 350 kJ/mol, respectively, for the same temperature range. Creep deformation in the siliconized silicon carbide below the threshold stress for creep damage was determined to be controlled by dislocation processes in the silicon phase. At applied stresses above the threshold stress for creep damage, creep damage enhanced the rate of deformation, resulting in an increased stress exponent and activation energy for creep. The contribution of creep damage to the deformation process was shown to increase the stress exponent from 4 to 10.

Daniel F. Carroll et. al. [4] in 1989 studied a technique for tensile creep testing of ceramics. An experimental technique for measuring tensile creep deformation in ceramic materials to temperatures of 1500°C is described. The technique uses simple flat dog-bone-shaped specimens and a hot-grip design for the loading fixture, which provide good alignment at minimum cost. Creep deformation is measured using laser extensometry to monitor the relative displacement of flags that are attached to the gauge section of the specimen.

Ching-Fong Chen et. al. [5] in 1990 studied an improved analysis for flexural creep with application to sialon ceramics. By using a statistical least-squares method to minimize the differences between predicted and measured load-point displacement rates from four-point bend specimens, power-law creep parameters for tension and compression were estimated. An alternative but simpler method of estimating power-law creep parameters from flexural creep data is also proposed. This method entails the direct measurements of steady-state creep strain rates at two stress levels by an

indentation technique. Based on a closed-form solution, the power-law creep parameters could then be estimated from both the measured neutral axis locations and curvature rates. The results from these two methods compare favorably with one another, and with the simple compressive creep data. Both methods yield a high stress exponent of about 14 for tension and a stress exponent of about unity for compression. Cavitation-enhanced creep in tension and diffusional creep in compression are responsible for this asymmetric behavior.

Ralph F. Krause Jr. et. al. [6] in 1992 studied the comparison of observed creep curvature rates to theoretical rates for both an alumina ceramic at 1000°C and a silicon nitride ceramic at 1200°C in four-point flexure. The observed rates have been calculated from published rise-displacement rates, and the theoretical rates have been calculated from published power-law parameters for compressive and tensile creep, which differ appreciably for these ceramics. Although both compressive and tensile creep measurements are easier to analyze than flexural creep measurements, the latter are usually less expensive and easier to conduct. The present work shows the usefulness of flexural creep tests to verify the accuracy of compressive and tensile creep tests.

Bernard J. Hockey et. al. [7] in 1992 studied the effect of microstructure on the creep of siliconized silicon carbide. Mechanisms of creep deformation have been investigated for a commercial grade of siliconized carbide containing 33%/silicon. Microstructural studies of both tensile and compressive test specimens indicate dislocation damage generation in both the silicon carbide and the silicon phases as a consequence of creep. In the silicon carbide, dislocation damage was normally restricted to contact sites between the silicon carbide grains resulting from high intergranular contact stresses during deformation. Dislocation damage was also observed in the silicon. Although dislocation damage was heavy in some regions of the specimens, most regions of the specimens, most regions were free of dislocations. This result is consistent with the hypothesis that deformations occurs by the motion of clusters of grains during deformation. In tension, creep at high strain rates, was accompanied by the formation of cavities at Si/SiC interfaces within the intergranular silicon phase. As cavities were not associated with dislocations, their growth was probably controlled by diffusional processes. Based on observations of the microstructure, a model of deformation is proposed to explain the fact that siliconized

silicon carbide creeps faster in tension than in compression, at the same applied stress. The model is based on soil mechanics concepts. It is suggested that creep is controlled by intergranular friction between aggregate particles of the composite.

John W. Holmes et. al. [8] in 1992 discussed an experimental technique for the elevated temperature tensile fatigue and creep testing of fiber-reinforced ceramics. The experimental approach utilizes edge-loaded specimens with rectangular gage-sections. Novel furnace and grip designs which allow testing in air to 1500°C are provided. The specimen, furnace and grip designs discussed in the paper have been successfully used to test unidirectional and cross-ply SiCf/ Si_3N_4, SiCf/SiC, Cf/SiC and SiCf/calcium-aluminosilicate composites.

C. J. Gasdaska et. al. [9] in 1994 studied tensile creep in an in situ-reinforced silicon nitride and suggested that a hyperbolic sine function of applied stress and temperature, which follows from Eyring's theory of the viscosity of fluids, describes the tensile creep behavior:

$$\dot{\varepsilon}_s = A_s T \sinh\left(\frac{\Omega_s \sigma}{RT}\right) \exp\left[-\frac{\Delta H_s}{RT}\right]$$

where Ω_s and ΔH_s are the apparent activation volume and energy, respectively. For stresses greater than ~50 MPa, Eq. simplifies to an exponential function

$$\dot{\varepsilon}_s = A_s T \exp\left[-\frac{\Delta H_s + \Omega_s \sigma}{RT}\right]$$

M. N. Menon et. al. [10] in 1994 studied creep and stress rupture behavior of an advanced silicon nitride and chose to capture the curvature of the $\log(\dot{\varepsilon}) - \log(\sigma)$ plot by expressing the data using a single apparent activation energy, but with different stress exponents at high and low stresses

$$\log_e \dot{\varepsilon}_s = A_M - \frac{Q_M}{RT} + a_2 \log_e \frac{\sigma}{E} + a_3 \sqrt{\left(\log_e \frac{\sigma}{E} - \tau\right)^2}$$

where E is Young's modulus, τ occurs at the transition between the two stress exponents, and a_2 and a_3 are constants such that at low stresses $\left(\log_e \frac{\sigma}{E} > \tau\right)$ the stress

exponent in a power law formulation is $n_{low}=a_2-a_3$, while at high stresses $\left(\log_e \frac{\sigma}{E} > \tau\right)$ it is $n_{high}=a_2+a_3$.

Tatsuki Ohji et. al. [11] in 1994 studied the tensile creep and crack growth behavior of silicon carbide doped with alumina at 1400°C. Excellent creep resistance was observed for stresses from 150 MPa to 200 MPa. From the creep exponent of 1.4 and the activation energy of 320 KJ/mol, the principal creep mechanism was Coble creep. The creep failure was caused by slow crack growth from a preexisting flaw. The crack was found to grow subcritically along grain boundaries almost in isolation. The relation between the time–to–failure and the applied stress was well treated by a diffusive crack growth model, and the threshold stress of this material at 1400°C was estimated at 165 MPa.

Jow-Lian Ding et. al. [12] in 1994 studied creep and creep rupture behavior of an advanced silicon nitride ceramic and systematically characterized in the temperature range 1150° to 1300°C using uniaxial tensile creep tests. Absence of tertiary creep and the order-of-magnitude breaks in both creep rate and rupture lifetime at certain threshold combinations of stress and temperature were two characteristic features of the creep behavior observed. Thermal annealing was found to have enhanced both subsequent creep resistance and creep rupture life. The stress exponent *(n)* and the activation energy *(Q)* defined in the Norton relation were found to be 12.6 and 1645 kJ/mol for the material investigated. Both values appear to fall in the general range of those reported for other but similar types of Si_3N_4 ceramic materials. The stress exponent, *m*, equivalent to the slope of the Larson–Miller equation was found to be in the range 13 to 14.4, and that defined as *p* in the Monkman–Grant relation to be 0.91, based on the available experimental data. The values of *m*, *n*, and *p* obtained above approximately support the interrelationship of the three exponents given by $p = m/n$.

Charles S. White et. al. [13] in 1995 studied notched tensile creep testing of ceramics. The use of axisymmetric tensile creep specimens containing semicircular notches is shown to provide important data which complement results of the common smooth tensile creep test. The notch provides a stress and strain concentration which can represent the non-uniform state of actual components in service. Finite element analysis confirms that the initial concentration of stress redistributes during creep to

yield a more uniformly loaded cross-section. Additionally, it is shown that the stress follows a highly non-proportional loading path during creep. The first experiments of notched tensile creep of a ceramic (silicon nitride) are examined in the light of finite element simulations of the transient deformation. The implications of notched tensile creep are discussed as an important test for the evaluation of constitutive models.

William E. Luecke et. al. [14] in 1997 discussed "Interlaboratory Verification of Silicon Nitride Tensile Creep Properties". Five laboratories tested NIST-supplied, pin-loaded, 76-mm-long tensile creep specimens at 1400^0C under a 150 MPa load using flag-based, laser extensometry. The laboratories reported failure time and strain and supplied the individual creep curves. Only one of the laboratories produced failure times that were significantly less than the others. It is likely that their reduced failure times resulted from small load calibration and test temperature errors. After steps were taken to ameliorate these problems, three additional tests yielded failure times that agreed with those of the other four laboratories. Although the times to failure from the four laboratories that initially agreed were statistically indistinguishable, their creep curves exhibited subtle differences. These differences probably arose because the laboratories used different gage length definitions. When they recalculated the creep curves to the same gage length definition, the differences between the four laboratories whose times to failure agreed, vanished. Although a number of the specimens exhibited edge chips, creep cracks, and obvious chemical interactions with the flags, the presence of these defects did not reduce the time or strain to failure.

C. W. Li et. al. [15] in 1997 studied microstructure and tensile creep mechanisms of an situ-reinforced silicon nitride to arrive at an inverse exponential form

$$\dot{\varepsilon}_s = A_{sm}\frac{\sigma^{2/3}}{T}\exp\left[-\frac{\Delta H_{sm}}{RT}\right]\exp\left[-\frac{L}{RT\sigma}\right]$$

where L is a term involving the height of the grain-boundary step on which Si_3N_4 molecules are attaching and the energy of the step per unit length.

Jacques Crampon et. al. [16] in 1997 studied compressive creep and creep failure of $8Y_2O_3/3Al_2O_3$-doped hot-pressed silicon nitride. The compressive creep properties of hot-pressed Si_3N_4 have been investigated in the temperature range of 1543–1603 K in

air. The stress exponent, n, of the power creep law was determined to be 1.5, and the activation energy was determined to be 650 KJ/mol. Transmission electron microscopy observations showed that grain-boundary sliding occurred with cavitation formation in the grain-boundary glassy phase. The quasi-steady-state creep results were consistent with that of the diffusion controlled solution–diffusion–precipitation creep mechanism, and the distinguished failure mechanism was cavitation creep damage controlled by the viscosity of the boundary glassy phase. The compressive creep failure time, obtained at 1573 K, in the stress range of 175–300 MPa, followed the Monkman–Grant relation, indicating that cavity growth was mainly controlled by the creep response of the material.

Ralph F. Krause et. al. [17] in 1999 studied tensile creep and rupture of silicon nitride and characterized the tensile creep, rupture lifetime, and cavitation behavior of a commercial, gas-pressure sintered silicon nitride in the temperature range 1150°C to 1400°C and stress range 70MPa to 400 MPa. They proposed that the tensile creep rate of silicon nitride is highly nonlinear with stress. They found that the majority of the primary creep is not recoverable. The best representation of the data is one where the creep rate depends exponentially on stress, rather than on the traditional power law. This representation also removes the need to break the data into high and low stress regimes. They observed that cavitation of the interstitial silicate phase accompanies creep under all conditions, and accounts for nearly all of the measured strain. These observations are consistent with a model where creep proceeds by the redistribution of silicate phase from cavitating interstitial pockets, accommodated by grain-boundary sliding of silicon nitride.

They estimated a secondary creep rate, $\dot{\varepsilon}$ by assuming that before the tertiary stage the strain, ε, increased with time, t:

$$\varepsilon = \dot{\varepsilon}_s t + \varepsilon_{pm}\left[1 - \exp(-t/\tau\right]$$

where ε_{pm} is a maximum primary creep strain and τ is a time constant.

They have developed a model for the creep of silicon nitride. In this model, the exponential-like dependence of creep rate on stress arises from the kinetics of the redistribution of silicate material from growing cavities through the interstitial volume

surrounding them. Increasing stress activates an ever-greater fraction of cavities, and increases the creep rate by reducing the distance for silicate redistribution. This model also leads to an exponential form:

$$\dot{\varepsilon}_s = A_c \sigma \exp - \left(\frac{Q_c}{RT} \right) \exp(B_c \sigma)$$

where A_c and Q_c have their usual meanings, and B_c is a term related to the density of potential sites for cavity formation.

Sheldon M. Wiederhorn et. al. [18] in 2000 studied comparison of tensile and compressive creep behavior in silicon nitride. The creep behavior of a commercial grade of Si_3N_4 was studied at 1350° and 1400°C. Stresses ranged from 10 to 200 MPa in tension and from 30 to 300 MPa in compression. In tension, the creep rate increased linearly with stress at low stresses and exponentially at high stresses. By contrast, the creep rate in compression increased linearly with stress over the entire stress range. Although compressive and tensile data exhibited an Arrhenius dependence on temperature, the activation energies for creep in tension, 715.3 ~ 22.9 kJ/mol, and compression, 489.2 ~ 62.0 kJ/mol, were not the same. These differences in creep behavior suggest that mechanisms of creep in tension and compression are different. Creep in tension is controlled by the formation of cavities. The cavity volume fraction increased linearly with increased tensile creep strain with a slope of unity. A cavitation model of creep, developed for materials that contain a triple-junction network of second phase, rationalizes the observed creep behavior at high and low stresses. In compression, cavitation plays a less important role in the creep process. The volume fraction of cavities in compression was; 18% of that in tension at 1.8% axial strain and approached zero at strains <1%.

Ralph F. Krause Jr. et. al. [19] in 2001 characterized the tensile creep behavior of a gas-pressure-sintered silicon nitride containing silicon carbide at temperatures between 1375° and 1450°C with applied stresses between 50 and 250 MPa. Individual specimens were tested at fixed temperatures and applied loads. Each specimen was pin-loaded within the hot zone of a split-tube furnace through silicon carbide rods connected outside the furnace to a pneumatic cylinder. The gauge length was measured by laser extensometry, using gauge markers attached to the specimen. Exponential functions of stress and temperature were fitted to represent the secondary

creep rate and the creep lifetime. This material was found to be more creep resistant than two other silicon nitride ceramics that had been characterized earlier by the same method of measurement as viable candidates for high-temperature service.

Tatsuki Ohji et. al. [20] in 2001 studied high-temperature reliability of advanced ceramics at National Industrial Research Institute of Nagoya. The work described high-temperature reliability, particularly creep and creep rupture behavior of three engineering ceramics-silicon nitride, silicon carbide, and alumina based silicon-carbide-particulate ceramics-which are considered the most potential candidates for the use of blades of high-efficiency ceramic gas turbine. The structural reliability of silicon nitride is very often limited due to the softening of glassy phases formed at grain boundaries. On the other hand, silicon carbide, which generally does not contain glassy phase at the grain boundaries, shows excellent creep resistance even at very high temperatures. Finally, it is shown that creep resistance of alumina can be markedly improved by dispersing nano-sized silicon carbide particles into the grain boundary. Because of their excellent resistance to tensile creep, advanced ceramics have become a leading candidate for use of high temperature structural applications such as turbine blades and nozzles.

William E. Luecke et. al. [21] in 2002 discussed "Results of an International Round-Robin for Tensile Creep Rupture of Silicon Nitride". Fourteen laboratories participated in an inter laboratory study to establish the within-and between-laboratory repeatability of tensile creep rupture of silicon nitride. In air at 1375°C at 200 MPa, the times to failure ranged over a factor of 50, and the minimum creep rates ranged over a factor of 20. Despite these large ranges, taken individually, no one laboratory stands out from any other; all produced equally acceptable data. Consumers of silicon nitride tensile creep data must accept this magnitude of variability in reported creep data. The wide variety of specimen shapes and sizes, gripping systems, extensometry techniques, and temperature measurement strategies makes it impossible to assign definitively the root cause of the variability. However, there was a significant specimen size effect. As a group, the small diameter specimens lasted roughly five times longer and crept three times more slowly than the large-diameter button head specimens. A possible interpretation of the origin of this difference is that the oxidizing conditions affected more of the volume of the small specimens during the test.

The above study reveals that lots of work is done in the field of creep failure mechanisms, deformations due to creep, effect of creep on tensile and compressive behavior of ceramics, effect of microstructure on creep characteristics of ceramics etc. All of the major work has been done experimentally. But a study was not developed for controlling the creep behavior and improving the tensile and compressive characteristics under creep conditions. Thus a mathematical model is developed for non-linear analysis in ceramics and an optimization technique for reducing the undesirable failure is aimed for improving the characteristics of material under creep.

CHAPTER 3
FEM FORMULATION

The Finite Element Method solution used for the development of creep represents a systematic procedure for the implementation of the theorem of Minimum Potential Energy. This theorem states, "Of all the displacement functions which satisfy the displacement boundary conditions and for which a compatible set of strains exist, the function which satisfies the equilibrium equations and the stress boundary conditions makes the potential energy an absolute minimum". The equilibrium equations for the total solid are obtained by matrix superposition of the individual element stiffness and load matrices, resulting in a system of linear algebraic equations. Thus, the finite element procedure has replaced the original set of differential equations of equilibrium by an equivalent set of algebraic equations. The solution of this set of algebraic equations represents the solution of the problem.

3.1 BASIC FINITE ELEMENT PROCEDURE

The potential energy (ϕ) for an elastic body is defined by

$$\phi = \frac{1}{2}\int_{vol} \sigma_{ij}\varepsilon_{ij}\,dV - \int_{vol} w_i B_i\,dV - \int_{A_P} w_i P_i\,dA_P \qquad (3.1)$$

where

$B_i =$ body forces

$P_i =$ applied surface tractions

$w_i =$ displacement within the element

$A_P =$ area over which the applied surface traction acts

Equation (3.1) written in matrix form becomes

$$\phi = \frac{1}{2}\int_{vol} [\varepsilon]^T [\sigma] dV - \int_{vol} \{w\}^T \{B\} dV - \int_{A_P} \{w\}^T \{P\} dA_P \qquad (3.2)$$

The finite element method of solution requires the definition of the potential energy for each of the elements (total number = M) making up the total solid and the potential energy of the entire solid is written as the sum of integrals over the volume and surface of each element.

$$\phi = \sum_{m=1}^{M} \left[\int_{vol} \frac{1}{2} [\varepsilon]^T [\sigma] dV - \int_{vol} \{w\}^T \{B\} dV - \int_{A_P} \{w\}^T \{P\} dA_P \right] \qquad (3.3)$$

To generate the element stiffness and load matrices it is necessary to assume a displacement field within each element usually in the form of polynomials. The assumed displacement field must satisfy compatibility between elements of the system. Symbolically the displacement $\{\omega\}$ within the element can be defined as

$$\{w\} = [e]\{b\} \qquad (3.4)$$

where $\{b\}$ denotes the generalized displacements and $[e]$ is a geometry matrix associated with the order of polynomial that has been selected. Evaluating the displacements $\{w\}$ at the nodal points permits one to solve for the generalized displacements in terms of the nodal displacements $\{u\}$.

$$\{b\} = [h]\{u\} \qquad (3.5)$$

The strains $\{\varepsilon\}$ within an element are obtained from equation (4) by appropriate differentiation

$$\{\varepsilon\} = [g]\{b\} \qquad (3.6)$$

The stresses at any point within an element for an elastic material are expressed by the following stress-strain relationship

$$\{\sigma\} = [c]\{\varepsilon\} - \{\tau\} \qquad (3.7)$$

where τ denotes the thermal effects.

Combining Equations (3.4), (3.5), (3.6), and (3.7) and substituting into Equation (3.3) gives the potential energy as a function of the nodal displacements.

$$\phi = \sum_{m=1}^{M} \left[\begin{array}{l} \frac{1}{2} \int_{vol} \{u\}^T [h]^T [g]^T [c][g][h][u] dV - \int_{vol} \{u\}^T [h]^T [g]^T \{\tau\} dV - \int_{vol} \{u\}^T [h]^T [e]^T \{B\} \\ - \int_{A_P} \{u\}^T [h]^T [e]^T \{P\} dA_P \end{array} \right] \qquad (3.8)$$

The potential energy is minimized by

$$\frac{\partial \phi}{\partial u_i} = 0 \qquad \text{for i = 1,2,……..N} \qquad (3.9)$$

where N is the total number of nodal point displacements. Performing the operations indicated in Equation (3.9) yields the following relationship for the equilibrium of the finite element system:

$$\phi = \sum_{m=1}^{M}\left[\int_{vol}[h]^T[g]^T[c][g][h][u]dV\right] = \sum_{m=1}^{M}\left[\int_{vol}\left([h]^T[g]^T\{\tau\}+[h]^T[e]^T\{B\}\right)dV\right] + \sum_{m=1}^{M}\left[\int_{A_P}\left([h]^T[e]^T\{P\}\right)dA_P\right]$$

(3.10)

or written in symbolic form

$$[K]\{u\} = \{Q\} \qquad (3.11)$$

$[K]$ represents the stiffness matrix for the complete finite element system given by the sum of the individual stiffness matrices :

$$[K] = \sum_{m=1}^{M}[k^m] \qquad (3.12)$$

The individual stiffness matrices are given by

$$[k]^m = \int_{vol}[h]^T[g]^T[c][g][h]dV \qquad (3.13)$$

The load vector $\{Q\}$ is defined by

$$\{Q\} = \sum_{m=1}^{M}\left(\{L^m\}+\{R^m\}\right) \qquad (3.14)$$

where $\{L\}^m$ represents the body force vector given by

$$\{L\}^m = \int_{vol}\left([h]^T[g]^T\{\tau\}+[h]^T[e]^T\{B\}\right)dV \qquad (3.15)$$

and $\{R\}^m$ represents the laod vector due to surface forces given by

$$[R]^m = \int_{A_P}\left([h]^T[e]^T\{P\}\right)dA_P \qquad (3.16)$$

Equation (3.11) represents the relationship between all nodal point force s and the corresponding nodal point displacements. After imposing the boundary conditions on Equation (3.11), the reduced stiffness matrix is inverted and the nodal point displacements obtained. Knowing the nodal point displacements permits the evaluation of the strains using Equations (3.5) and (3.6). Equation (3.7) then permits the calculation of stresses corresponding to these strains. These results represent the complete solution to the elasticity problem.

3.2 MAHEMATICAL MODEL FOR CREEP

Inclusion of creep behavior forces the consideration of nonlinear stress-strain relationships. Substitution of the non-linear stress-strain relationships into the governing field equations for the system results in a set of nonlinear equations. Two methods of analysis are currently used for the solution of nonlinear problems:

1) Direct iteration procedure: Final solution is achieved by an iterative solution of the non-linear equations.
2) Incremental procedure: Final solution is achieved by solving a number of linearized problems distributed between the initial and final configuration.

The incremental procedure has been selected in the present case as it is completely general and provides a description of intermediate states. Furthermore, the incremental procedure is more easily adapted to the use of arbitrary forms of the creep law. The fundamental assumption in the incremental creep solution technique is that the time can be subdivided into sufficiently small time intervals such that the stress can be assumed to be constant with in each time interval. If this assumption is valid, then the nonlinear creep problem can be solved as a series of linear problems for each time interval treating the incremental creep strains from the last time interval as initial strains for the current time interval. Thus, for the incremental creep solution technique it becomes necessary to express all the relationships in incremental form.

First, assume the total change in strain during a time interval as the sum of the changes in the elastic $\{\Delta\varepsilon^E\}$ and creep strains $\{\Delta\varepsilon^C\}$

$$\{\Delta\varepsilon\} = \{\Delta\varepsilon^E\} + \Delta\varepsilon^C \qquad (3.17)$$

The incremental form of Hooke's law for an elastic body relates the change inelastic strains to the incremental stresses.

$$\{\Delta\sigma\} = [E]\left(\Delta\varepsilon^{E}\right) \qquad (3.18)$$

Combining Equations (3.17) and (3.18) yields the relationship between incremental stress, incremental total strain, and incremental creep strain.

$$\{\Delta\sigma\} = [E]\left(\{\Delta\varepsilon\} - \{\Delta\varepsilon^{C}\}\right) \qquad (3.19)$$

Combining Equations (3.5) and (3.6) and rearranging in incremental form gives the incremental strain - displacement relation,

$$\{\Delta\varepsilon\} = [g][h]\{\Delta u\} \qquad (3.20)$$

The incremental relationships for the equilibrium Equations (3.11) can be written in the following manner where the load vector $\{Q\}$ has been replaced by the incremental creep forces $\{\Delta F^{C}\}$ resulting from the incremental creep strains occurring during the previous time interval

$$\Delta u = [K]^{-1}\{\Delta F^{C}\}$$

where $\{\Delta F^{C}\} = [M]\{\Delta\varepsilon^{C}\}$ (3.21)

$[M]$ = matrix consisting of geometry and material properties

The specific form of the incremental creep law depends upon the material and environmental conditions, but its general functional form can be represented by the following equation

$$\{\Delta\varepsilon^{C}{}_{e}\} = \{f\left(\sigma_{e}, \varepsilon^{C}{}_{e}, t, \tau\right)\} \qquad (3.22)$$

where

$\{\varepsilon^{C}{}_{e}\}$=effective creep strain

With the above incremental relationships defined, the creep solution proceeds as follows:

1) Solve the elastic problem for the initial time (t=0) and determine the elastic stress distribution.
2) Assume for a small increment of time (Δt), that the stress remain constant. From the assumed creep law (Equation 3.22), which will be an empirical relationship experimentally determined, calculate the incremental change in effective creep strain. The formulation in terms of effective stress and strain permits the use of uniaxial creep data.
3) From the effective incremental creep strains calculate a set of fictitious incremental creep forces $\{\Delta F^C\}$.
4) Substitute the fictitious incremental creep forces into Equation (3.21) equivalent to resolving the elastic problem with the original load vector replaced with this set of forces. This step assures equilibrium of the system after the creep associated with time $\{\Delta t\}$ has occurred.
5) Substitute the incremental nodal displacements $\{\Delta u\}$ into Equation (3.20) to determine the total change in strain $\{\Delta \varepsilon\}$.
6) The incremental stresses $\{\Delta \sigma\}$ may now be computed from equation (3.19).
7) Add the incremental stresses $\{\Delta \sigma\}$ arising from the fictitious incremental creep forces to the initial elastic stresses to give the new stress distribution.
8) Repeat the procedure for the next time increment using the new stress distribution.

The basic assumptions used in the derivation of the finite element stiffness relations are:

1) The material is isotropic, homogeneous, and has identical creep properties in tension and compression.
2) Displacements and strains are assumed small so that small deformation theory is applicable.
3) Solution at time (t =0) is entirely elastic and no time independent plastic strains are considered.
4) System is assumed to creep at constant external load, and unloading is not considered.

3.3 PLANE STRESS ANALYSIS

The basic stiffness element used for the plane stress analysis will be a triangular element of unit thickness oriented in the r-z plane as shown in Figure 3.1.

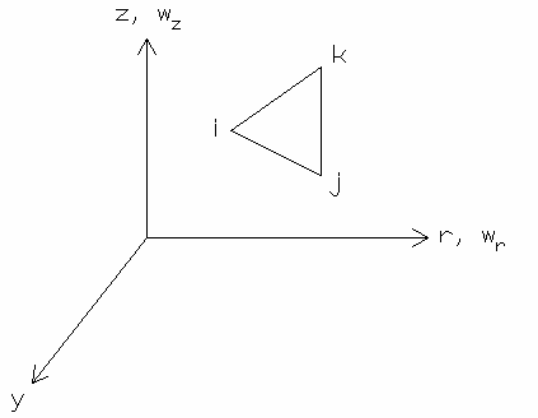

Fig 3.1: Basic Stiffness Element for Plane Stress Analysis

The displacement field is assumed to be a linear polynomial in the (r,z) coordinates. Equation (3.4) in matrix form becomes

$$\begin{Bmatrix} \omega_r(r,z) \\ \omega_z(r,z) \end{Bmatrix} = \begin{bmatrix} 1 & r & z & 0 & 0 & 0 \\ 0 & 0 & 0 & 1 & r & z \end{bmatrix} \begin{Bmatrix} b_1 \\ b_2 \\ b_3 \\ b_4 \\ b_5 \\ b_6 \end{Bmatrix} \tag{3.23}$$

Evaluating the displacements at the nodal points permits one to solve for the generalized displacements $\{b\}$ in terms of the nodal displacements $\{u\}$

$$\{b\} = [h]\{u\} \tag{3.24}$$

where

$$[h] = \frac{1}{\beta} \begin{bmatrix} r_j z_k - r_k z_j & 0 & r_k z_i - r_i z_k & 0 & r_i z_k - r_j z_i & 0 \\ z_j - z_k & 0 & z_k - z_i & 0 & z_i - z_j & 0 \\ r_k - r_j & 0 & r_i - r_k & 0 & r_j - r_i & 0 \\ 0 & r_j z_k - r_k z_j & 0 & r_k z_i - r_i z_k & 0 & r_i z_k - r_j z_i \\ 0 & z_j - z_k & 0 & z_k - z_i & 0 & z_i - z_j \\ 0 & r_k - r_j & 0 & r_i - r_k & 0 & r_j - r_i \end{bmatrix}$$

and $\beta = r_i(z_j - z_k) + r_j(z_k - z_i) + r_k(z_i - z_j)$ (3.25)

The strain - displacement relations in rectangular coordinates are given by

$$\varepsilon_{rr} = \frac{\partial \omega_r}{\partial r};\ \varepsilon_{zz} = \frac{\partial \omega_z}{\partial z};\ \gamma_{rr} = \frac{\partial \omega_r}{\partial z} + \frac{\partial \omega_z}{\partial r} \tag{3.26}$$

Equation (3.6) for the strains becomes

$$\begin{Bmatrix} \varepsilon_{rr} \\ \varepsilon_{zz} \\ \gamma_{rz} \end{Bmatrix} = \begin{bmatrix} 0 & 1 & 0 & 0 & 0 & 0 \\ 0 & 0 & 0 & 0 & 0 & 1 \\ 0 & 0 & 1 & 0 & 1 & 0 \end{bmatrix} \begin{Bmatrix} b_1 \\ b_2 \\ b_3 \\ b_4 \\ b_5 \\ b_6 \end{Bmatrix} \tag{3.27}$$

For this case the stress-strain relationships for an isotropic material are given by:

$$\sigma_{yy} = \sigma_{ry} = \sigma_{zy} = 0 \tag{3.28}$$

where y is the coordinate axis normal to the r-z plane. Thus, equation in matrix form becomes

$$\begin{Bmatrix} \sigma_{rr} \\ \sigma_{zz} \\ \sigma_{rz} \end{Bmatrix} = \frac{E}{1-\upsilon^2} \begin{bmatrix} 1 & \upsilon & 0 \\ \upsilon & 1 & 0 \\ 0 & 0 & \frac{(1-\upsilon^2)}{(1+\upsilon)} \end{bmatrix} \begin{Bmatrix} {\varepsilon_{rr}}^E \\ {\varepsilon_{zz}}^E \\ {\varepsilon_{rz}}^E \end{Bmatrix} \tag{3.29}$$

To obtain the stress-strain relationships for the creep problem, the total strain ε_{ij} is assumed to be composed of an elastic strain ${\varepsilon^E}_{ij}$,creep strain ${\varepsilon^C}_{ij}$ and a thermal strain $(\alpha \Delta T)$.

$$\varepsilon_{ij} = {\varepsilon^E}_{ij} + {\varepsilon^C}_{ij} + \delta_{ij} \alpha \Delta T \tag{3.30}$$

In matrix form, the elastic strain is given by

$$\{\varepsilon^E\} = \{\varepsilon\} - \{\varepsilon^C\} - \{\alpha \Delta T\} \tag{3.31}$$

Substituting the appropriate form of Equation (3.31) into Equation (3.29) and imposing the assumption that the creep strains are incompressible $\left(\varepsilon^{C}{}_{kk}=0\right)$ yields the following stress-strain relationship:

$$\begin{Bmatrix}\sigma_{rr}\\ \sigma_{zz}\\ \sigma_{rz}\end{Bmatrix}=\frac{E}{\left(1-\upsilon^{2}\right)}\begin{bmatrix}1 & \upsilon & 0\\ \upsilon & 1 & 0\\ 0 & 0 & \frac{\left(1-\upsilon^{2}\right)}{\left(1+\upsilon\right)}\end{bmatrix}\begin{Bmatrix}\varepsilon_{rr}\\ \varepsilon_{zz}\\ \varepsilon_{rz}\end{Bmatrix}-\frac{E}{\left(1-\upsilon^{2}\right)}\begin{bmatrix}1 & \upsilon & 0\\ \upsilon & 1 & 0\\ 0 & 0 & \frac{\left(1-\upsilon^{2}\right)}{\left(1+\upsilon\right)}\end{bmatrix}\begin{Bmatrix}\varepsilon^{C}{}_{rr}\\ \varepsilon^{C}{}_{zz}\\ \varepsilon^{C}{}_{rz}\end{Bmatrix}-\frac{E\alpha\Delta T}{\left(1-\upsilon\right)}\begin{Bmatrix}1\\ 1\\ 0\end{Bmatrix} \tag{3.32}$$

Symbolically

$$\{\sigma\}=[A]\{\varepsilon\}-[D]\{\varepsilon^{C}\}-\{\varepsilon^{\tau}\} \tag{3.33}$$

Combining Equations (3.23), (3.24), (3.25), (3.27) and (3.33), and substituting into Equation (3.3) gives the potential energy expression which is minimized with respect to the nodal displacements resulting in the following equilibrium equations written in incremental form

$$[K]\{\Delta u\}=\{\Delta F^{C}\} \tag{3.34}$$

$$\{\Delta F^{C}\}=\int_{vol}[h]^{T}[g]^{T}\{D\}\{\Delta\varepsilon^{C}\}dV \tag{3.35}$$

Since all of the quantities under the integral sign are constant within each element including the incremental creep strains, it is possible to write Equation (3.34) in the form of Equation (3.21).

$$\{\Delta u\}=[K]^{-1}[M]\{\Delta\varepsilon^{C}\} \tag{3.36}$$

where $[M]=[h]^{T}[g]^{T}[D]\int_{Area}dA$. The volume integral reduces to an area integral since the triangular element was assumed to have unit thickness.

Upon selecting the specific form of the incremental creep law to be used, it is possible to define the incremental creep strains

$$\begin{Bmatrix} \Delta\varepsilon^{C}{}_{rr} \\ \Delta\varepsilon^{C}{}_{zz} \\ \Delta\varepsilon^{C}{}_{rz} \end{Bmatrix} = \frac{\Delta\varepsilon^{C}{}_{e}}{2\sigma_e} \begin{Bmatrix} 2\sigma_{rr} - \sigma_{zz} \\ 2\sigma_{zz} - \sigma_{rr} \\ 3\sigma_{rz} \end{Bmatrix} \tag{3.37}$$

where $\sigma_e = \sqrt{\sigma^2{}_{rr} - \sigma_{rr}\sigma_{zz} + \sigma^2{}_{zz} + 3\sigma^2{}_{rz}}$

Thus, the incremental form of Equation (3.27), corresponding to Equation (3.20), together with Equations (3.36) and (3.37) represent the incremental relationships needed to solve the plane stress creep problem.

3.4 PLANE STRAIN ANALYSIS

The plane strain analysis uses the same basic stiffness element as used for the plane stress analysis shown in Figure 3.3. The difference between the plane stress and plane strain analysis concerns the specific form of the stress-strain relationship. For the plane strain case the following conditions are assumed:

$$\varepsilon_{yy} = \sigma_{ry} = \sigma_{zy} = 0 \; ; \; \varepsilon^{C}{}_{yy} = 0 \tag{3.38}$$

Thus, the equation specialized to the plane strain case becomes in matrix form,

$$\begin{Bmatrix} \sigma_{rr} \\ \sigma_{zz} \\ \sigma_{rz} \end{Bmatrix} = \frac{E}{(1+\upsilon)(1-2\upsilon)} \begin{bmatrix} (1-\upsilon) & \upsilon & 0 \\ \upsilon & (1-\upsilon) & 0 \\ 0 & 0 & (1-2\upsilon) \end{bmatrix} \begin{Bmatrix} \varepsilon_{rr}{}^{E} \\ \varepsilon_{zz}{}^{E} \\ \varepsilon_{rz}{}^{E} \end{Bmatrix} \tag{3.39}$$

To satisfy the condition $\varepsilon_{yy} = 0$, the stress normal to the plane of the triangular element is given by,

$$\sigma_{yy} = \upsilon(\sigma_{rr} + \sigma_{zz}) \tag{3.40}$$

Substituting the appropriate form of Equation (3.31) into Equation (3.39) and assuming that the creep strains are incompressible $\varepsilon^{C}{}_{kk} = 0$ yields the following stress-strain relationships:

$$\begin{Bmatrix} \sigma_{rr} \\ \sigma_{zz} \\ \sigma_{rz} \end{Bmatrix} = \frac{E}{(1+\upsilon)(1-2\upsilon)} \begin{bmatrix} (1-\upsilon) & \upsilon & 0 \\ \upsilon & (1-\upsilon) & 0 \\ 0 & 0 & (1-2\upsilon) \end{bmatrix} \begin{Bmatrix} \varepsilon_{rr} \\ \varepsilon_{zz} \\ \varepsilon_{rz} \end{Bmatrix} - \frac{E}{(1+\upsilon)(1-2\upsilon)}$$

$$\begin{bmatrix} (1-\upsilon) & \upsilon & 0 \\ \upsilon & (1-\upsilon) & 0 \\ 0 & 0 & (1-2\upsilon) \end{bmatrix} \begin{Bmatrix} \varepsilon^{C}{}_{rr} \\ \varepsilon^{C}{}_{zz} \\ \varepsilon^{C}{}_{rz} \end{Bmatrix}$$

(3.41)

Comparing Equations (3.32) and (3.41) it is apparent that the plane stress equations can be converted to plane strain equations through the following material property transformations:

$$E_1 = \frac{E}{(1-\upsilon^2)} \; ; \; \upsilon_1 = \frac{\upsilon}{(1-\upsilon)} \; ; \; \alpha_1 = \alpha(1+\upsilon) \tag{3.42}$$

Thus, to solve a plane strain problem the material properties are modified by Equation (3.42) and substituted into the plane stress solution routine. The resultant solution corresponds to the solution for the plane strain problem.

The other modifications necessary for the plane strain problem are associated with the incremental creep strains. For the plane stress case, $\sigma_{yy} = 0$, but for the plane strain case σ_{yy} is given by Equation (40). Therefore, the incremental strains are given by

$$\begin{Bmatrix} \Delta\varepsilon^C{}_{rr} \\ \Delta\varepsilon^C{}_{zz} \\ \Delta\varepsilon^C{}_{rz} \end{Bmatrix} = \frac{\Delta\varepsilon^C{}_e}{2\sigma_e} \begin{Bmatrix} (2-\upsilon)\sigma_{rr} - (1+\upsilon)\sigma_{zz} \\ (2-\upsilon)\sigma_{zz} - (1+\upsilon)\sigma_{rr} \\ 3\sigma_{rz} \end{Bmatrix} \tag{3.43}$$

where

$$\sigma_e = \sqrt{\sigma^2{}_{rr} - \sigma_{rr}\sigma_{zz} + \sigma^2{}_{zz} - 2\upsilon(1-\upsilon)\sigma_{rr}\sigma_{zz} + 3\sigma^2{}_{rz}} \tag{3.44}$$

Note that the value used for Poisson's ratio (υ) should be the initial value before transformation. Since the initial material properties for the plane strain case will be the transformed values, Equations (3.44) should be written in terms of the transformed value of Poisson's ratio (υ_1).

$$\begin{Bmatrix} \Delta\varepsilon^C{}_{rr} \\ \Delta\varepsilon^C{}_{zz} \\ \Delta\varepsilon^C{}_{rz} \end{Bmatrix} = \frac{\Delta\varepsilon^C{}_e}{2\sigma_e} \begin{Bmatrix} \left[\frac{(2+\upsilon_1)}{(1+\upsilon_1)}\right]\sigma_{rr} - \left[\frac{(1+2\upsilon_1)}{(1+\upsilon_1)}\right]\sigma_{zz} \\ \left[\frac{(2+\upsilon_1)}{(1+\upsilon_1)}\right]\sigma_{zz} - \left[\frac{(1+2\upsilon_1)}{(1+\upsilon_1)}\right]\sigma_{rr} \\ 3\sigma_{rz} \end{Bmatrix}$$

(3.45)

where

$$\sigma_e = \sqrt{\sigma^2{}_{rr} - \sigma_{rr}\sigma_{zz} + \sigma^2{}_{zz} - \left[(2\upsilon_1)/(1+\upsilon_1)^2\right]\sigma_{rr}\sigma_{zz} + 3\sigma^2{}_{rz}}$$

Thus, to solve a plane strain problem it is necessary to replace Equation (3.37) in the plane stress routine with Equation (3.45) and modify the material properties using Equation (3.42). The resultant solution from the plane stress routine corresponds to the solution for the plane strain problem.

3.5 TIME INCREMENT SELECTION

The success of the incremental procedure for solving creep problems depends upon the ability to select appropriate time intervals. In turn, the time intervals selected depend upon the specific form of the creep law that is used. Thus, it is necessary to compute the desired time increments.

As an example consider the following creep law:

$$\Delta\varepsilon^C{}_e = C10^{MT}\sigma^n{}_e\Delta t \tag{3.46}$$

where C, *M*, *n* are constants with different materials

T = temperature (^{0}F)
t = time (hr)

Since the first step in the incremental procedure is to solve the elastic problem, the elastic values for the effective strain are known for each of the triangular finite elements

$$\varepsilon^E{}_e = \frac{1}{E}\sigma_e \tag{3.47}$$

Thus, the initial time increment can be found by setting the initial incremental effective creep strain equal to a fraction (η_0) of the maximum value for the effective elastic strain.

$$\varepsilon^{C}{}_{e} = \eta_0 \left(\varepsilon^{E}{}_{e}\right)\max \tag{3.48}$$

Substituting Equations (3.46) and (3.47) into (3.48) gives the following values for the initial time increment.

$$\Delta t_1 = \eta_0 \sigma_e^{(1-n)} / 10^{MT} CE \tag{3.49}$$

The specific value used for η_0 depends upon the particular problem. The above limiting conditions restrict η_0 to fall within the following range

$$1/25 \le \eta_0 \le 1/10$$

Subsequent time intervals will be computed on the basis of the fractional change in maximum effective stress allowed per time interval

$$\Delta t_{i+1} = \left(\Delta t_i\right)\eta / \left(\Delta\sigma_e / \sigma_e\right)_{\max} \quad (\text{ i = 1,2,}\ldots\ldots\ldots\ldots\ ) \tag{3.50}$$

where η= assumed fractional change in stress allowed for each time interval. For each problem, η must be selected keeping in mind that time increments are chosen sufficiently small such that the stresses may be assumed to be constant within each time interval. Experience has shown that η should fall within the following range.

$$0.03 \le \eta \le 0.10$$

One further limiting condition is placed upon the time interval selection $\eta / \left(\Delta\sigma_e / \sigma_e\right)_{\max} \le D$ where D is a constant ranging in values from 1.2 to 2.0 depending upon the specific problem. This condition restricts the maximum increase in the time increment for any time interval and is imposed to assure convergence of the solution.

CHAPTER 4
RESULTS AND DISCUSSIONS

Figure 4.1 describes the original design of the tensile creep specimen geometry. The specimen geometry is shown in terms of total length *TL*; pin-hole size *D*; neck radius *R*; head width *W*; and gage length *GL*. The dimensions of the specimen are: 50.00 mm total length, 2.00 mm thickness, 20.00 mm gauge length, 12.5 mm head width, 4.76 mm pinhole diameter, and 2.50 mm neck radius. A constant load is applied to the specimen from the pinhole (pin-loaded).

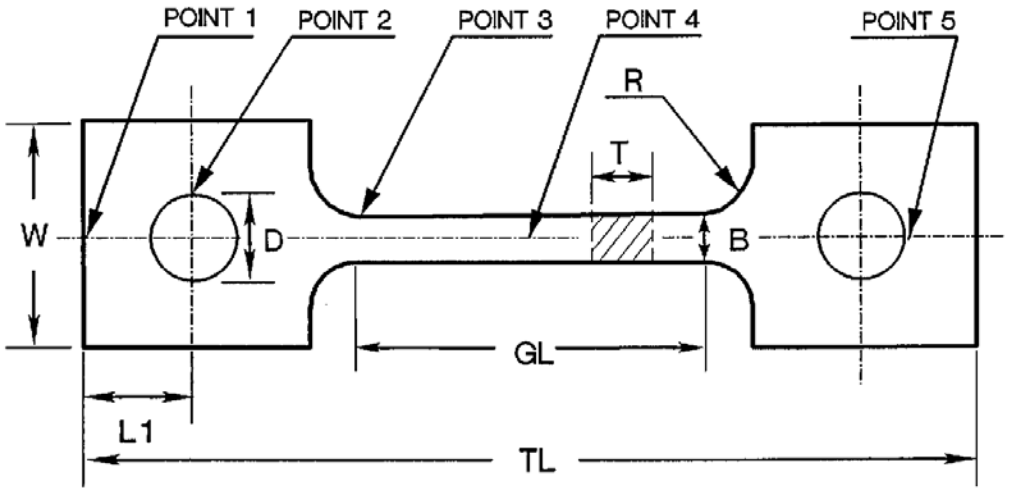

Fig 4.1: Initial design of the tensile creep specimen

Point 1: Head stress concentrator; Point 2: Hole stress concentrator; Point 3: Neck stress concentrator; Point 4: Gage section; Point 5: Load point

The material selected for study is a grade of commercially available Silicon Nitride or Silicon Carbide. Its mechanical properties at ambient temperature are as follows:

For Silicon Nitride

Modulus of elasticity, *E* = 350 Gpa
Poisson's ratio, y = 0.24
Ultimate tensile strength, *S*u = 900 Mpa
Weibull modulus = 15

For Silicon Carbide

Modulus of elasticity, *E* = 400 Gpa
Poisson's ratio, y = 0.24
Ultimate tensile strength, *S*u = 500 Mpa
Weibull modulus = 17

The objective of the present work is to study the effect of creep stress and strain in an adopted ceramic tensile specimen. Using the mathematical model discussed in the last chapter, a program code in C/C++ is developed for the analysis of the specimen. The code is then extended to include the non-linear effect arising for creep by the use of incremental procedure.

Here a two-part design analysis is presented. In the first part, the stress and strain fields around the pin hole caused by the contact between the pin and the specimen is analyzed. This will help to understand the cause of premature failure for many specimens of original design, and plan our design path in the second part of the analysis. In the second part, the geometry is altered systematically to minimize the stress/strain at the critical spots, thereby yielding the final design for the optimized geometry.

Throughout the entire design procedure, the total length of the specimen is fixed. This condition is regarded as given, and is the only constraint imposed on the problem. All other parameters are varied to find the optimum dimensions. In the optimization process, the current design parameters as shown in Fig.4.1 are taken, except the pinhole diameter, as the initial values in the iterative optimization procedure. Throughout the entire creep analysis, since the applied load is kept constant, the nominal tensile stress in the gauge section is always maintained at 100 MPa.

In the optimum calculations, the following design criteria are followed in each iterative loop:

- Smallest stress concentration in the neck area (i.e. the transition region from the neck of the flange to the gauge section).
- Tensile stresses as high as possible in the loading pin rod, but without failures.
- Smallest critical stresses in the head.
- Longest possible gauge length.

4.1 ELASTIC STRESSES IN THE SPECIMEN

The specimen was analyzed using program code for various design parameters.

a) ***Design by hole stress:*** Taking a series of hole stresses against head width (*W)*, we obtain Fig. 4.2(a). If an allowable value of hole stress is specified for the specimen design, we can then determine the *W* value. In the same way, we get another group of values of hole stresses from Fig. 4.2(b) for a range of hole locations and determine the optimum value of hole position *L*1. By the same token, Fig. 4.2(c) is a plot of hole stress for a range of gage lengths, and the best gage length can then be determined from this plot. It turns out that the stresses are monotonically increasing for increasing gage lengths. For the sake of minimizing stress, the smallest gage length should be used. However, to fully utilize the material, the longest gage length should be adopted. Clearly a balance must be struck between these two opposing ‘‘forces’’. Similarly, Fig. 4.2(d) plots the hole stresses with increasing neck radius.

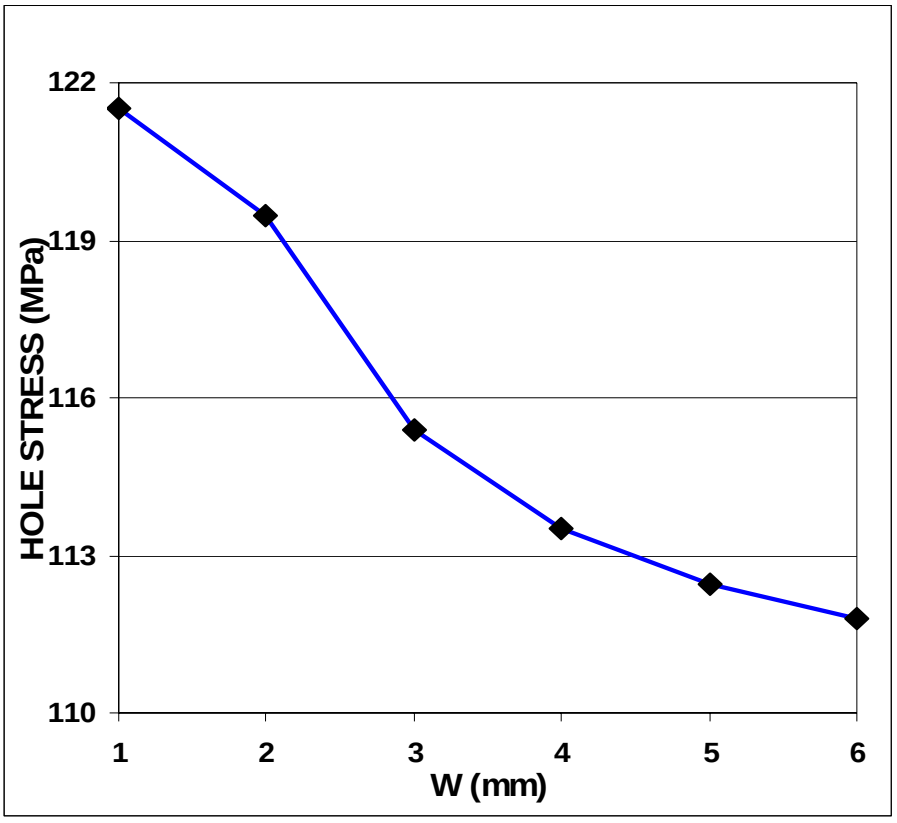

Fig. 4.2(a): Hole stress of the specimen as a function of head width W

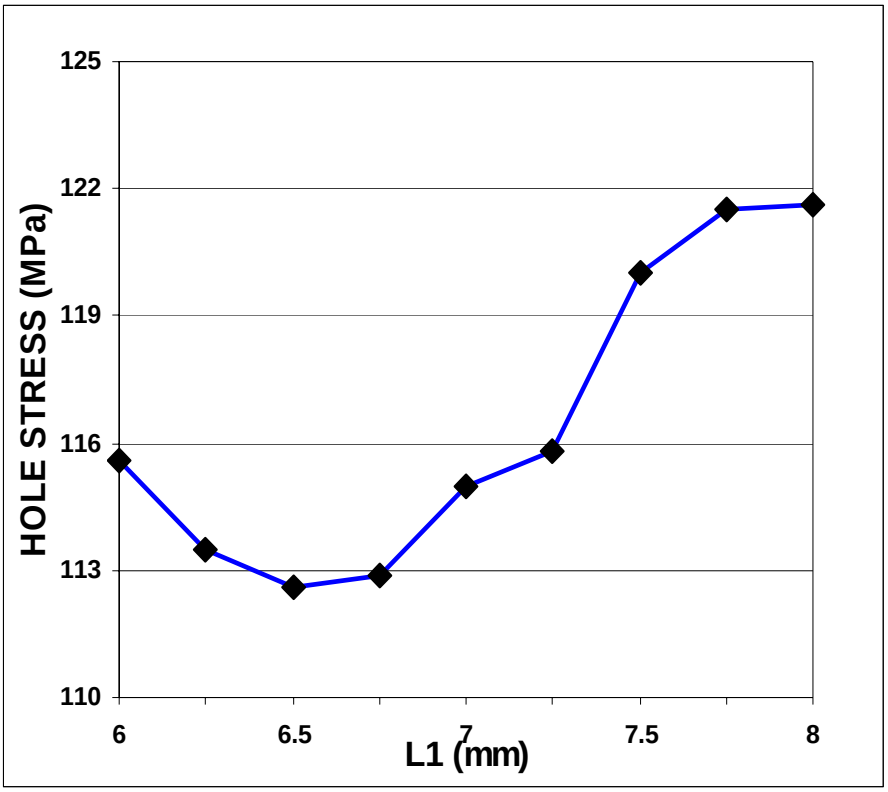

Fig. 4.2(b): Hole stress of the specimen as a function of hole location L1

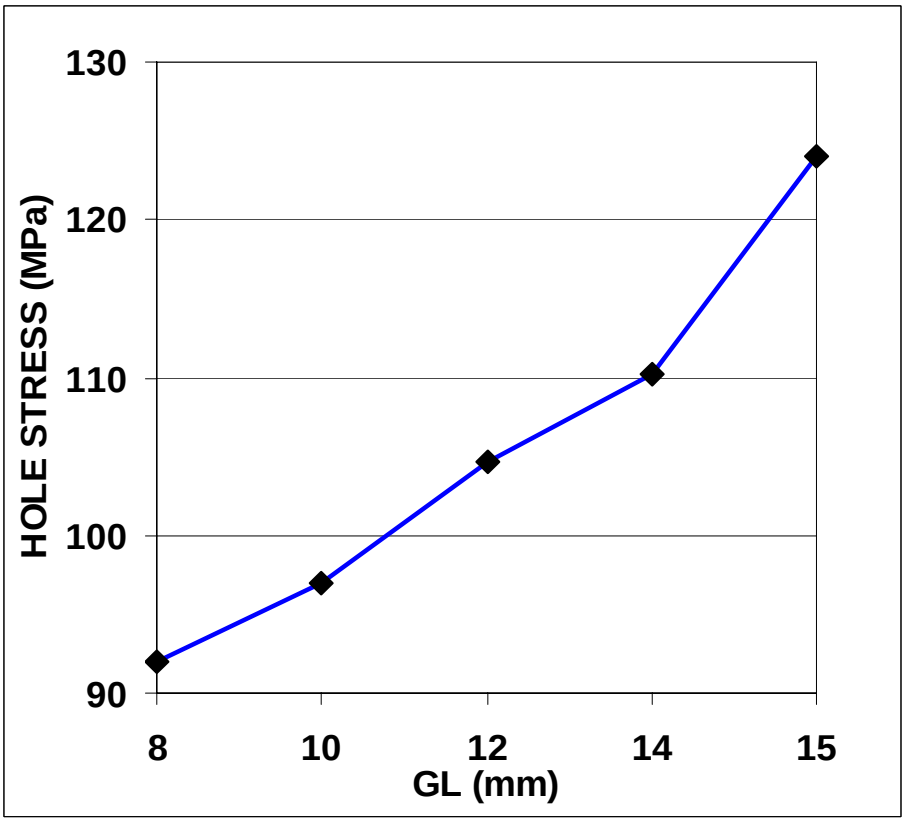

Fig. 4.2(c): Hole stress of the specimen as a function of gage length GL

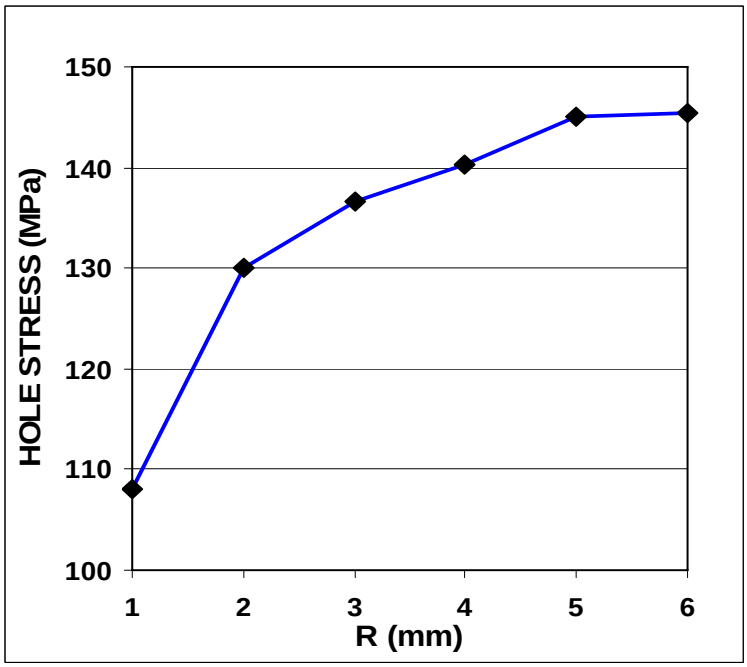

Fig. 4.2(d): Hole stress of the specimen as a function of neck radius R

b) ***Design by head stress:*** For a given value of pinhole diameter D = 4.76 mm, Fig. 4.3(a) shows the relationship between head stress and hole position $L1$. The head length $2 \times L1$ can be easily chosen from Fig. 4.3(a), if an allowable value of the head stress is imposed for the design. Similarly, Fig. 4.3(b) plots the head stress vs head width W for the given D, and the optimum value of W can thus be chosen.

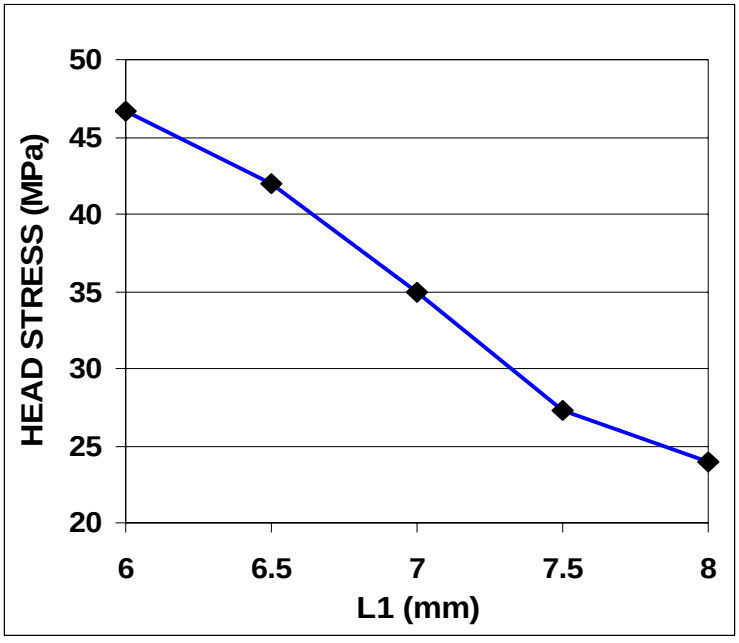

Fig. 4.3(a): Head stress of the specimen as a function of hole location L1

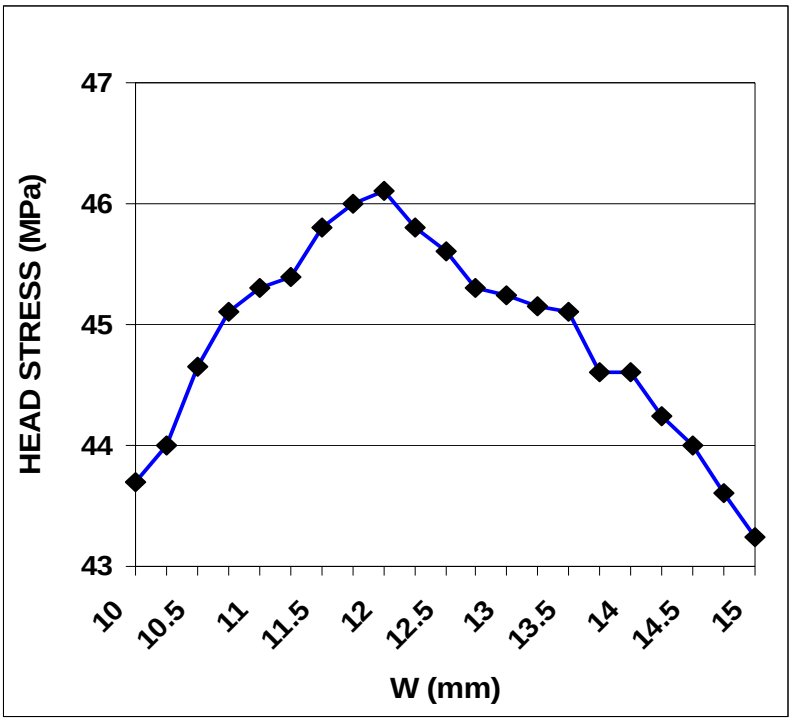

Fig. 4.3(b): Head stress of the specimen as a function of head width W

a) ***Design by neck stress:*** From Fig. 4.4, we find that the neck stress is strongly dependent upon the value of the neck radius *R*, so that if the allowable value of the neck stress is given in the design, the neck radius can be determined accordingly.

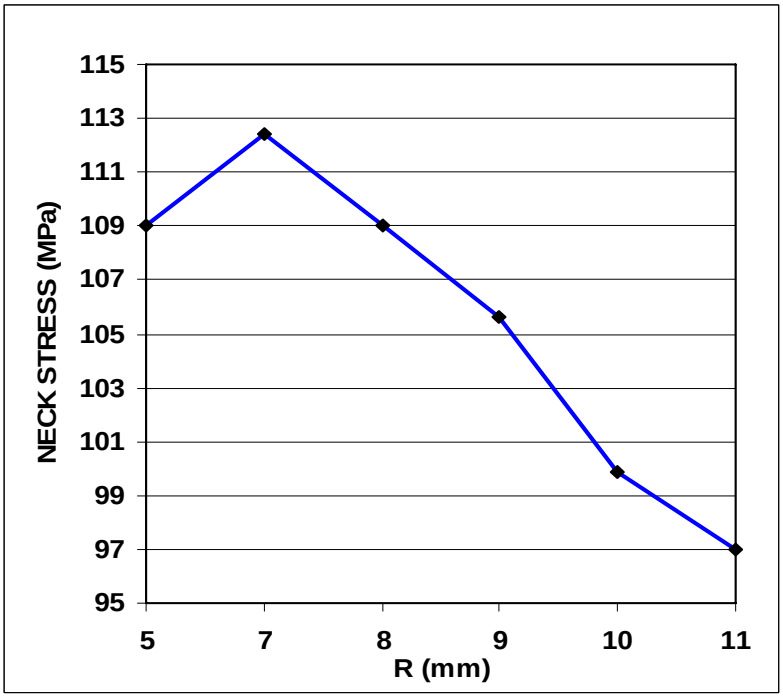

Fig. 4.4: Neck stress of the specimen as a function of neck radius R

4.2 VALIDATION

To validate the code, the tensile ceramic specimen was analyzed using the commercially available software, ANSYS. The specimen is discritisized as shown in Fig. 4.5. The specimen was analyzed without including creep characteristics. The equivalent stress distribution when a tensile force is applied keeping 100 MPa stress in the gauge length of specimen is shown in Figs. 4.6 and 4.7.

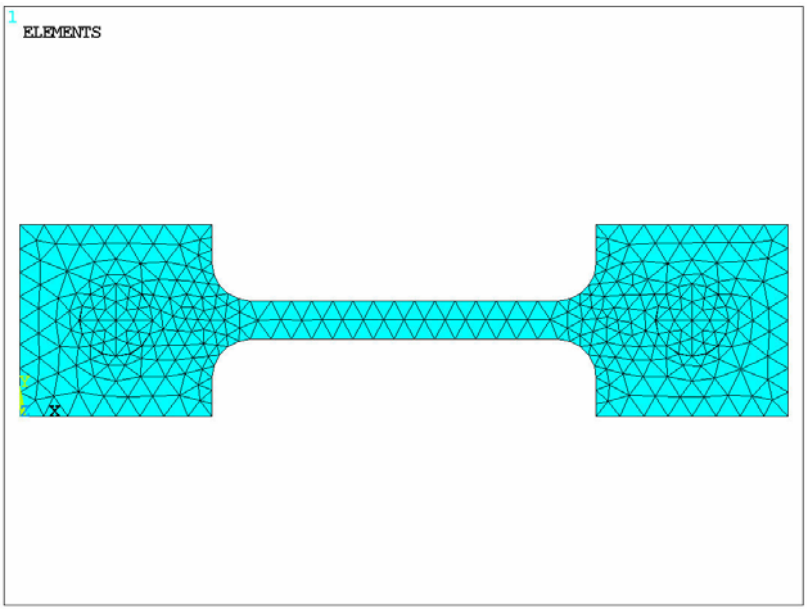

Fig 4.5: Initial specimen (Meshed)

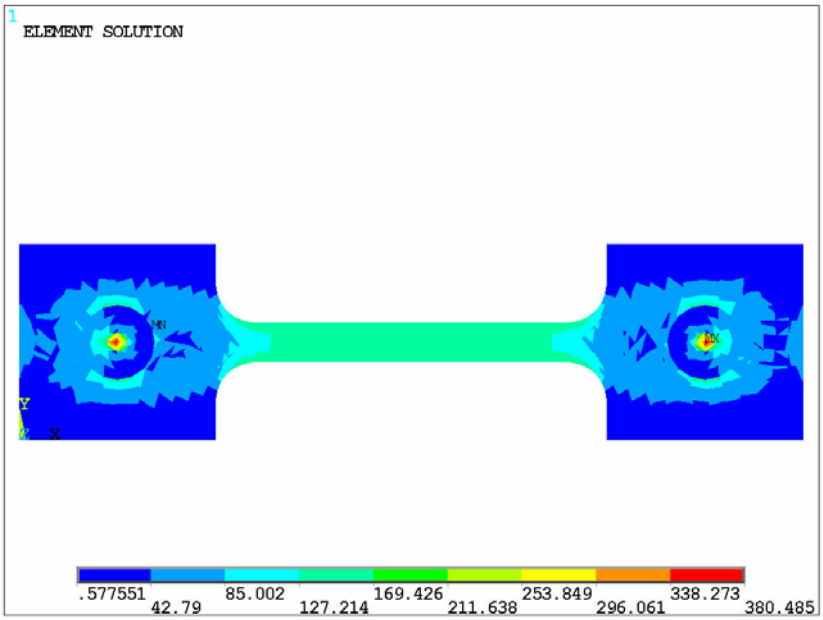

Fig 4.6: Equivalent Stress Distribution from the Contact Analysis (Including Pins)

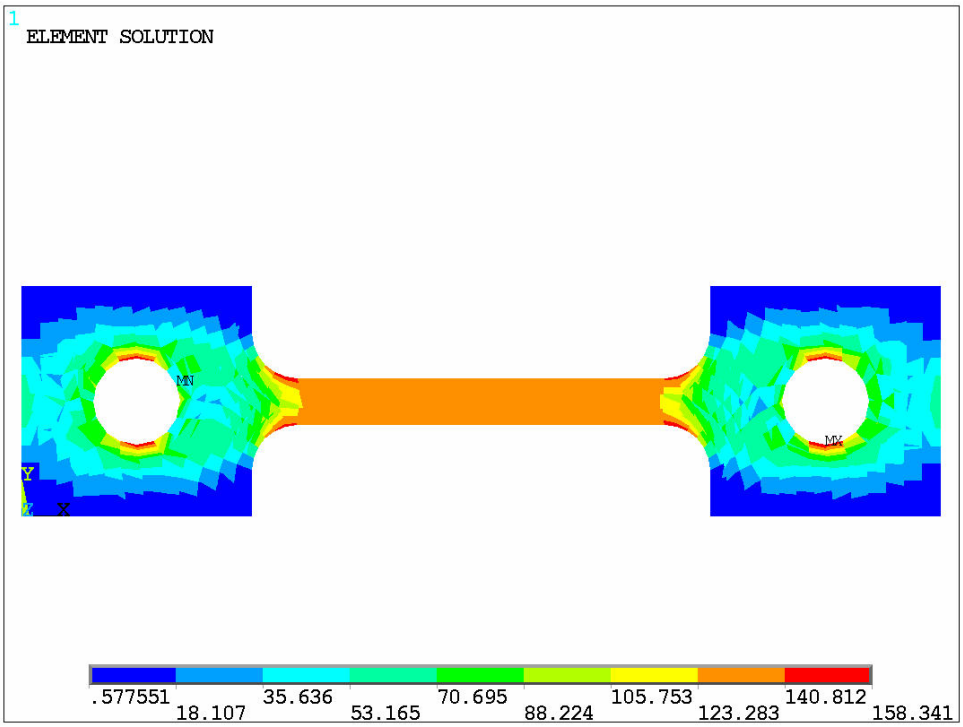

Fig 4.7: Equivalent Stress Distribution from the Contact Analysis (Excluding Pins)

The results obtained through program code are then compared with those from ANSYS. Figs. 4.8-4.14 shows fair matching of the results.

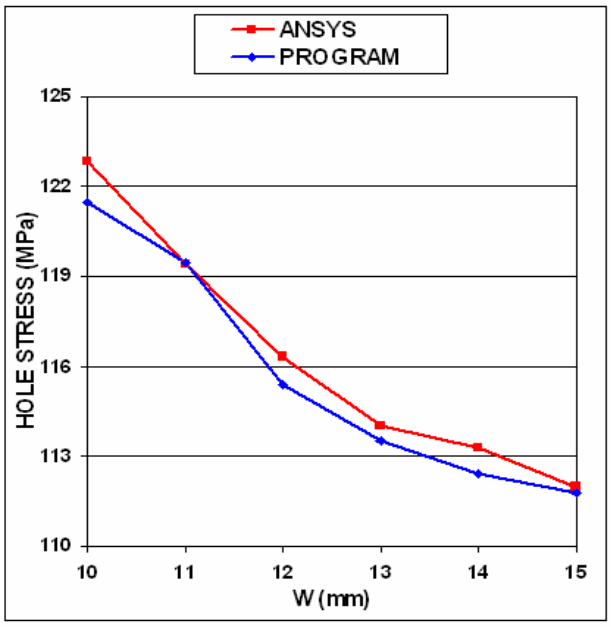

Fig. 4.8: Comparison of hole stress as a function of neck radius R (ANSYS vs program)

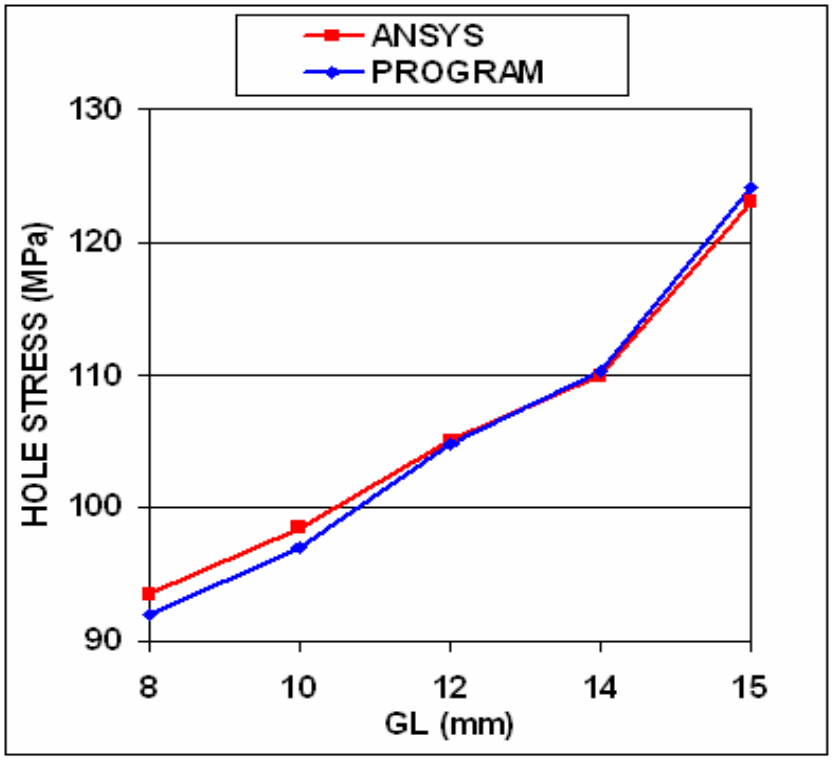

Fig. 4.9: Comparison of hole stress as a function of gauge length GL (ANSYS vs program)

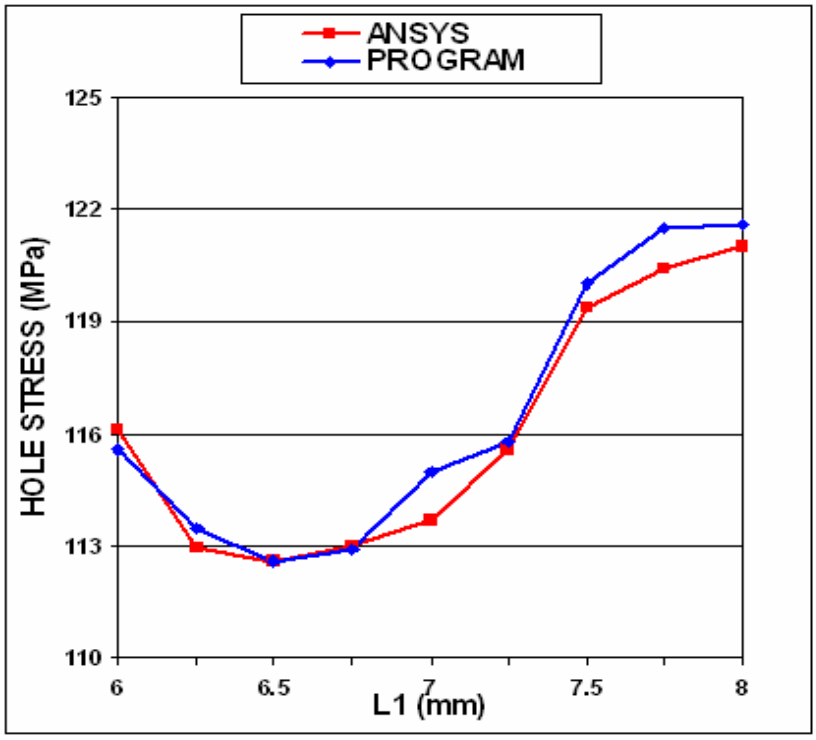

Fig. 4.10: Comparison of hole stress as a function of hole location L1 (ANSYS vs program)

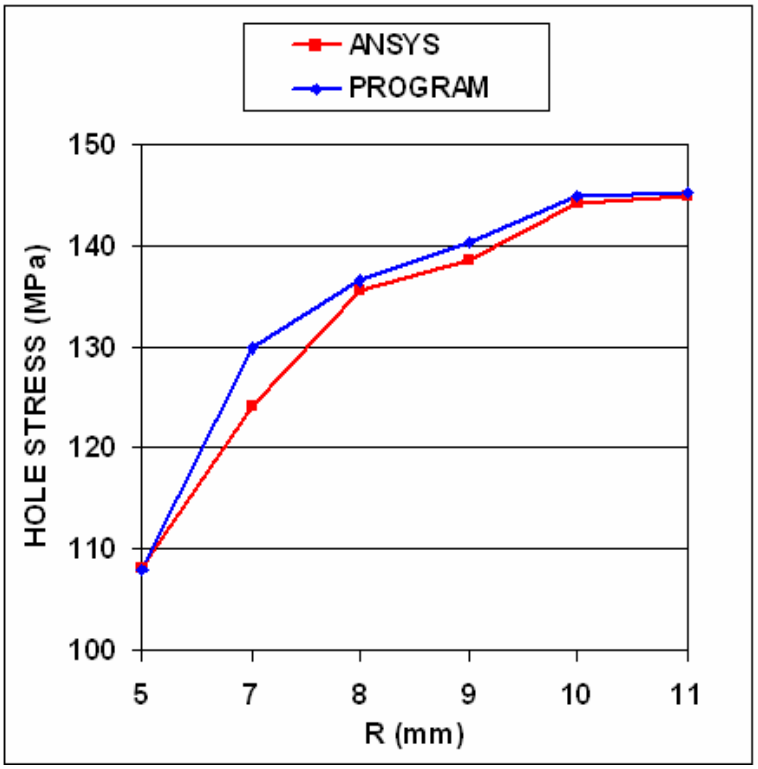

Fig. 4.11: Comparison of hole stress as a function of neck radius R (ANSYS vs program)

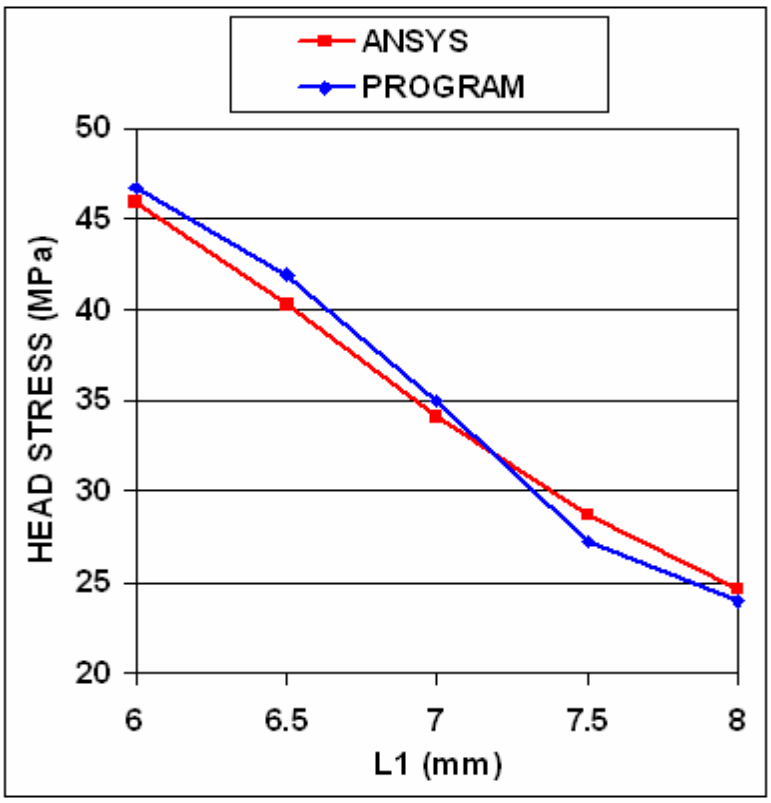

Fig. 4.12: Comparison of head stress as a function of hole location L1 (ANSYS vs program)

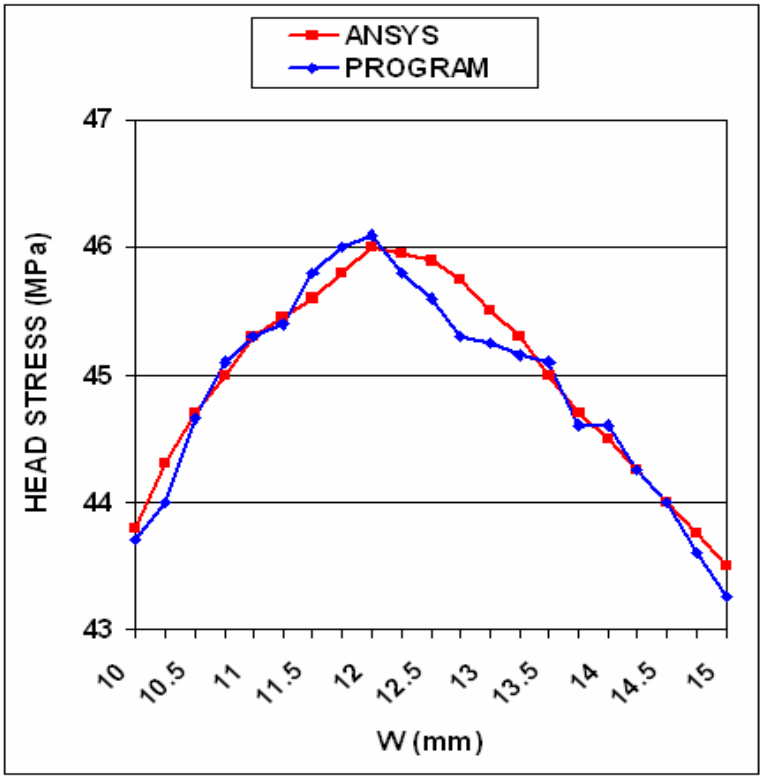

Fig. 4.13: Comparison of head stress as a function of head width W (ANSYS vs program)

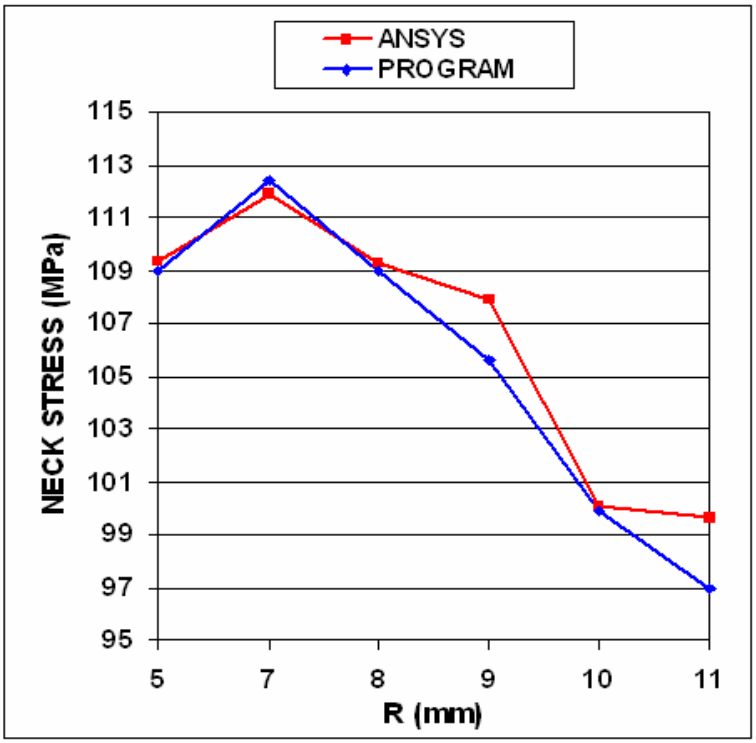

Fig. 4.14: Comparison of neck stress as a function of neck radius R (ANSYS vs program)

4.3 ALLOWABLE STRESSES

The specimen is then optimized using ANSYS for the allowable stress values. A series of criteria is considered for the optimum design, including the allowable value of hole stress $\sigma^c{}_{hole}$ on the edge of the pinhole, the allowable value of head stress $\sigma^c{}_{head}$, and also the allowable value of neck stress $\sigma^c{}_{neck}$. The design criteria are expressed as follows:

$$\sigma_{hole} \leq \sigma^c{}_{hole}$$

$$\sigma_{head} \leq \sigma^c{}_{head}$$

$$\sigma_{neck} \leq \sigma^c{}_{neck}$$

where σ_c is the allowable stress. In the optimum design, the following criterion is set after taking the allowable stress values into account for the selected silicon nitride:

$$\sigma^c{}_{hole} = 115 \text{ Mpa}$$

$$\sigma^c{}_{head} = 100 \text{ MPa}$$

$$\sigma^c{}_{neck} = 110 \text{ MPa}$$

The following set of design parameters are then obtained as the optimum design for a 50 mm total length specimen after a series of iterations:

D = 4.76 mm

W = 12.5 mm

R = 8 mm

L1 = 7.25 mm

GL = 14.5 mm

The optimum design specimen with meshing is as shown in Fig. 4.15

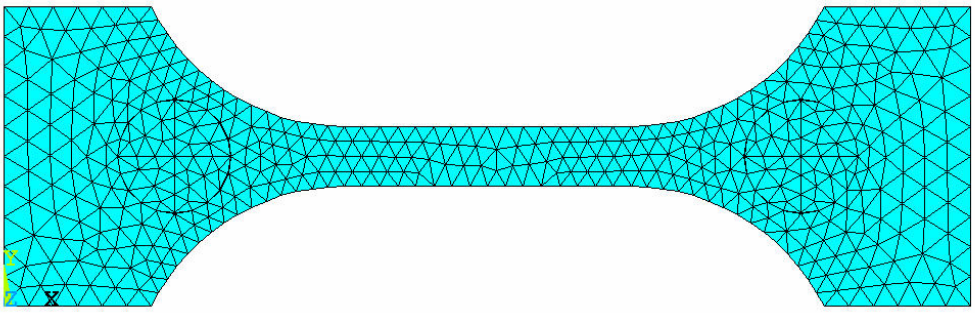

Fig 4.15: Optimum Designed Specimen

4.4 ELASTIC STRESSES IN OPTIMUM DESIGN

Analysis results of the elastic stress distributions in the case of the optimum design for a 50 mm specimen are shown in Figs. 4.16 and 4.17.

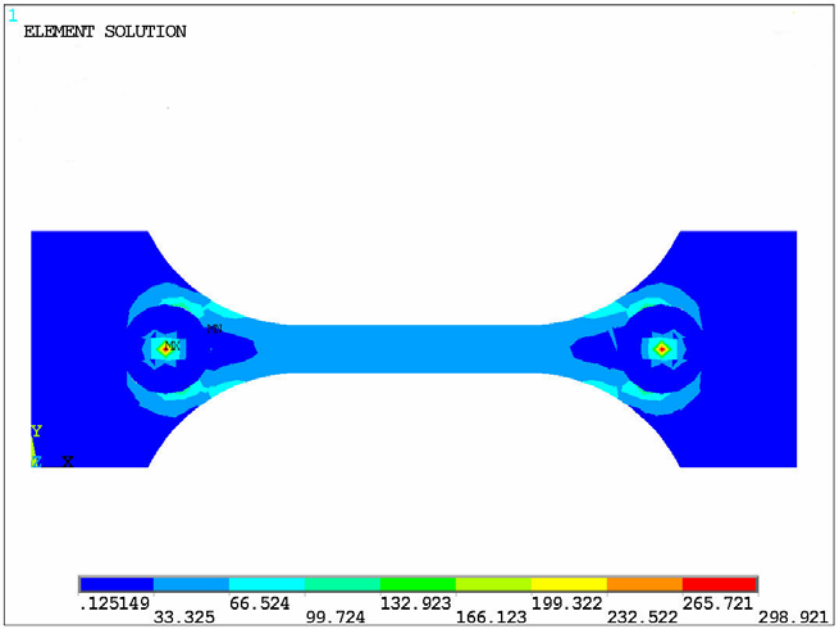

Fig 4.16: Equivalent stress distribution in optimum design from contact analysis (including pins)

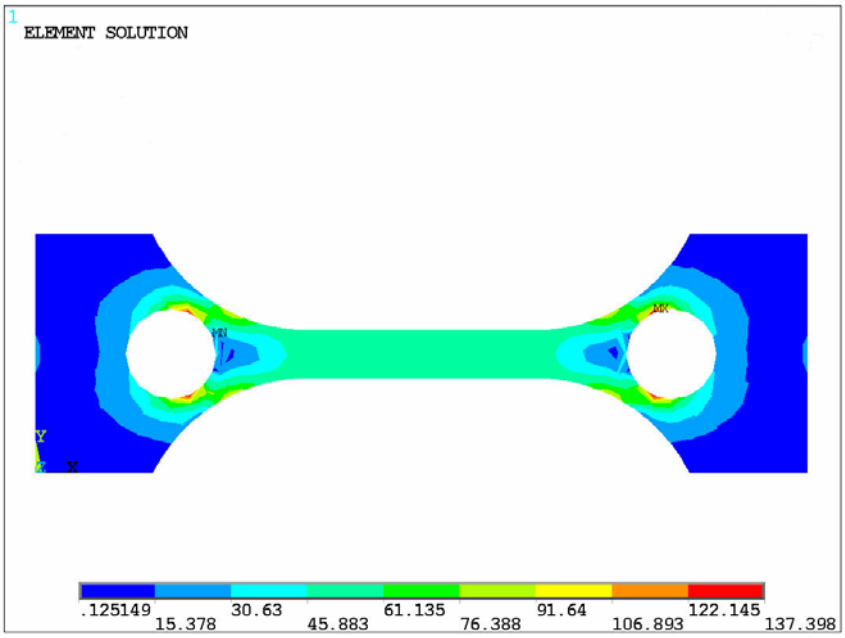

Fig 4.17: Equivalent stress distribution in optimum design from contact analysis (excluding pins)

4.5 CREEP BEHAVIOUR

The work was then extended for creep behavior in both original and optimized specimen using ANSYS and program code. The stress redistribution contour for the initial specimen due to creep from ANSYS is displayed in Figs. 4.18-4.20. At the early stage of creep, the stress near the hole edge is high but drops dramatically with time.

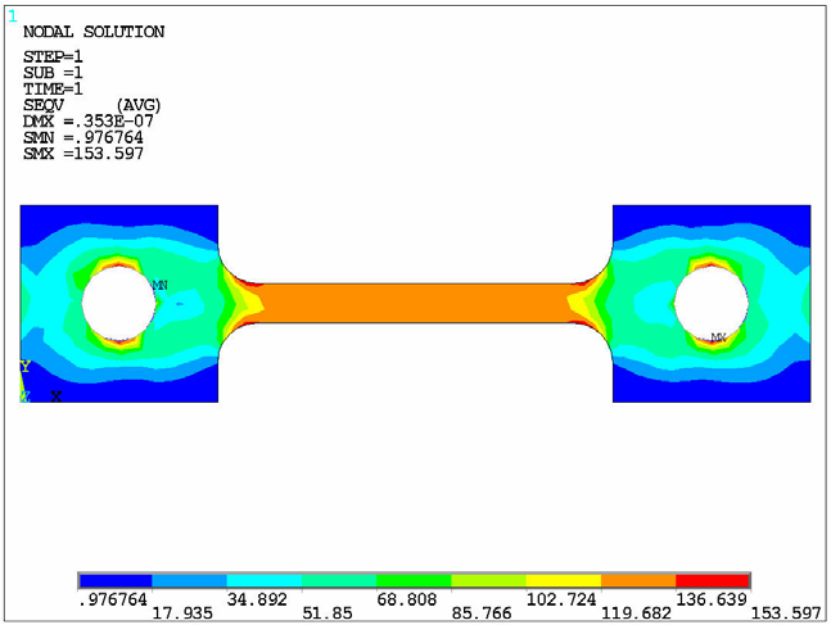

Fig 4.18: Creep stress redistribution: Equivalent stress at t=1

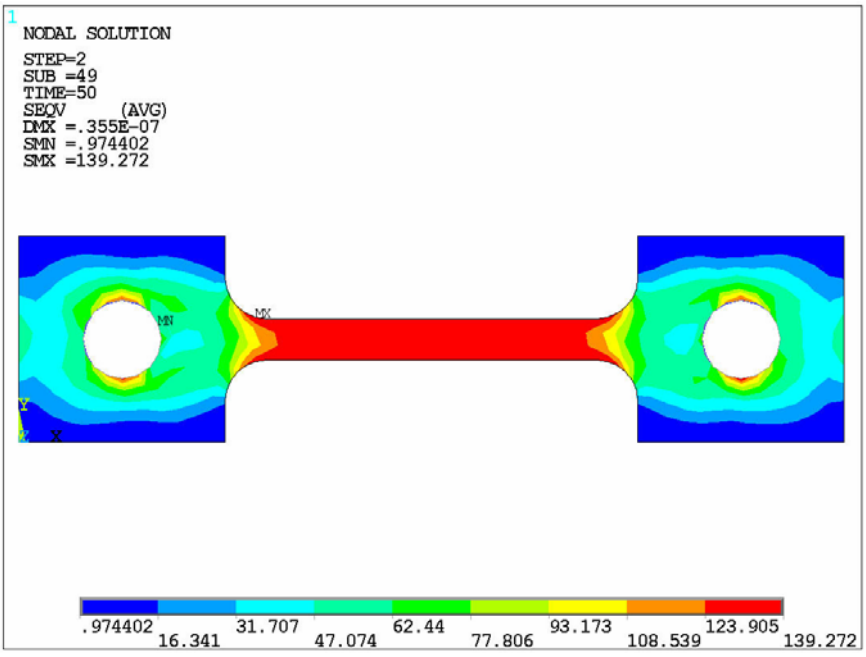

Fig 4.19: Creep stress redistribution: Equivalent stress at t=50

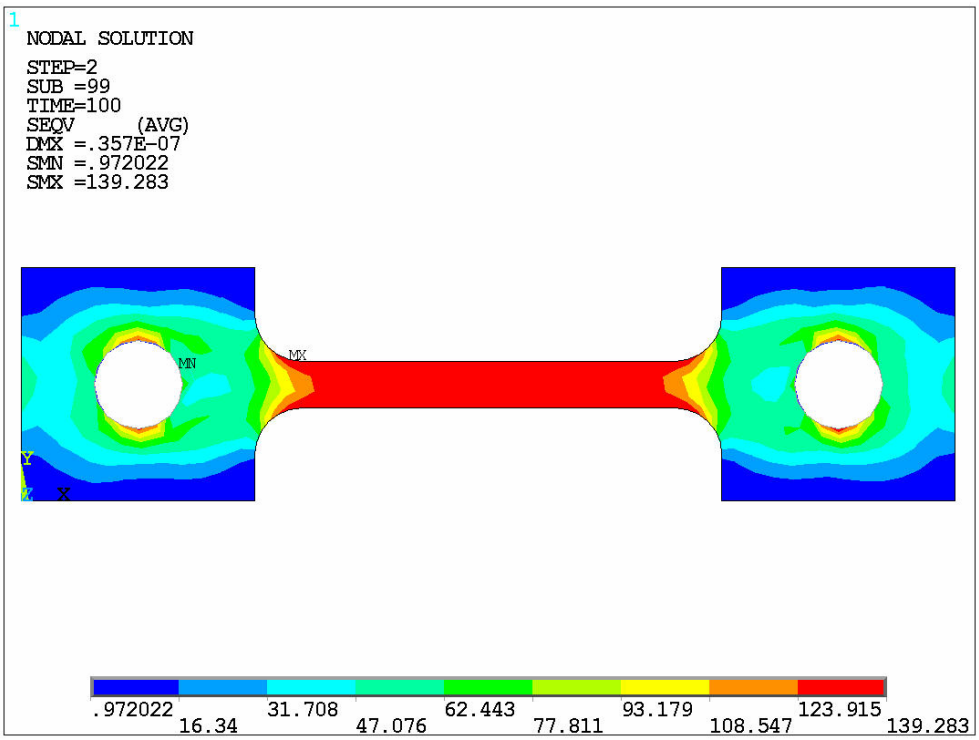

Fig 4.20: Creep stress redistribution: Equivalent stress at t=100

The stress redistribution contour for the final specimen due to creep is displayed in Figs. 4.21-4.23.

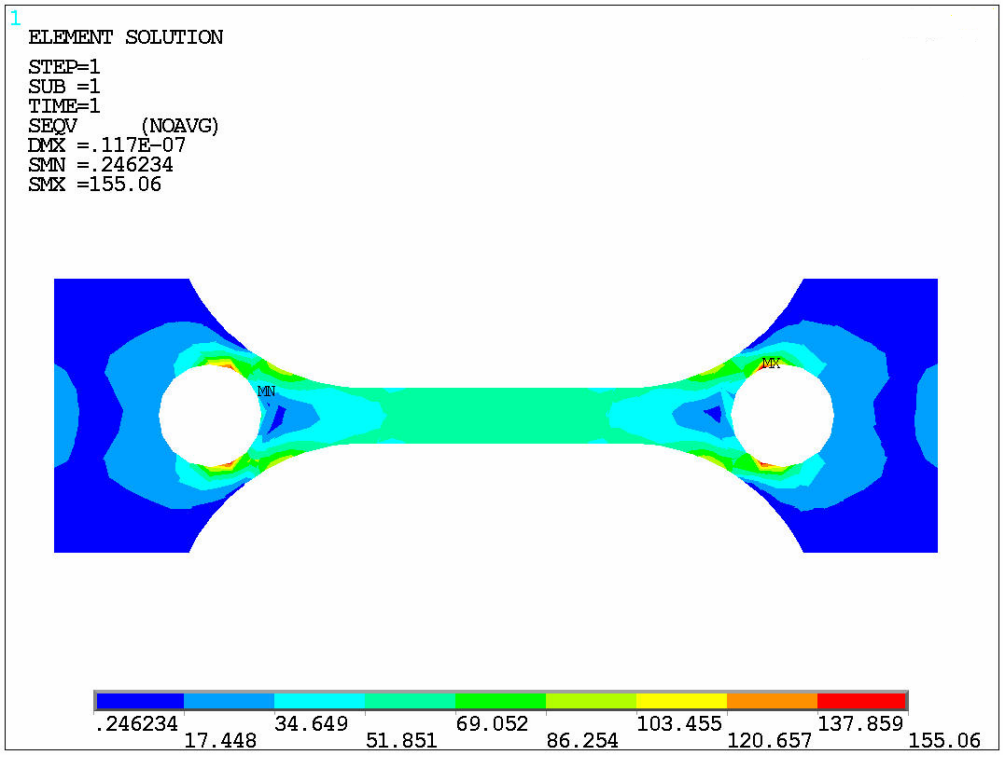

Fig 4.21: Creep stress redistribution: Equivalent stress at t=1

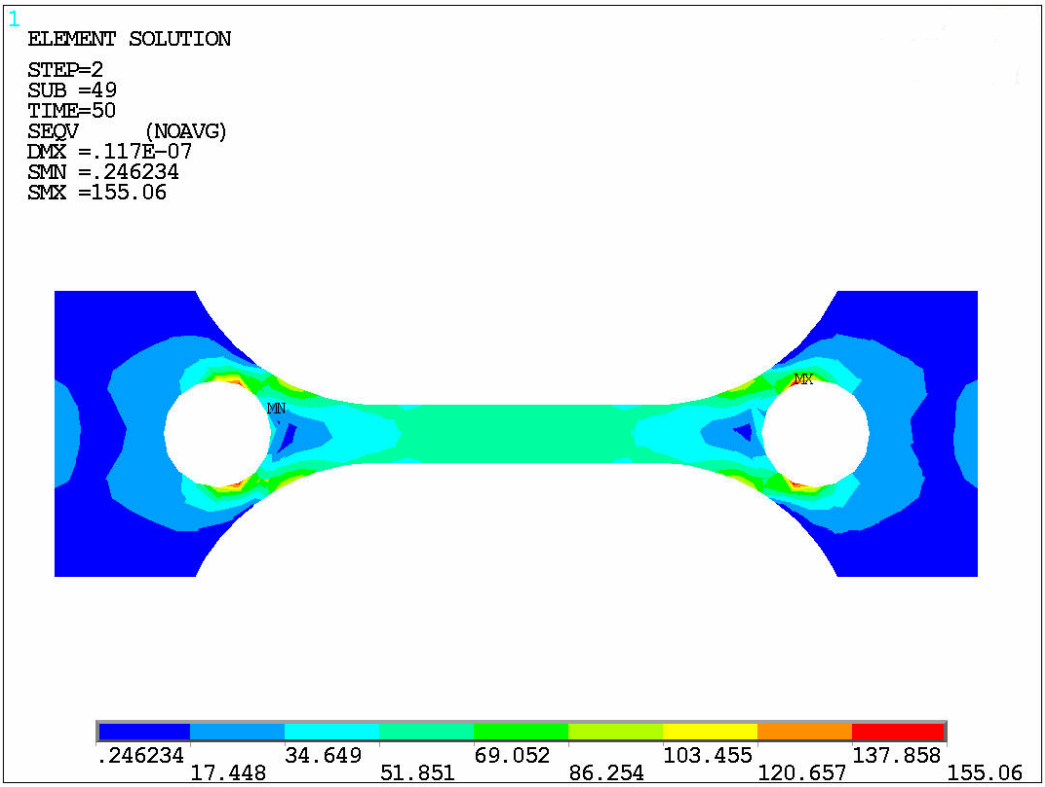

Fig 4.22: Creep stress redistribution: Equivalent stress at t=50

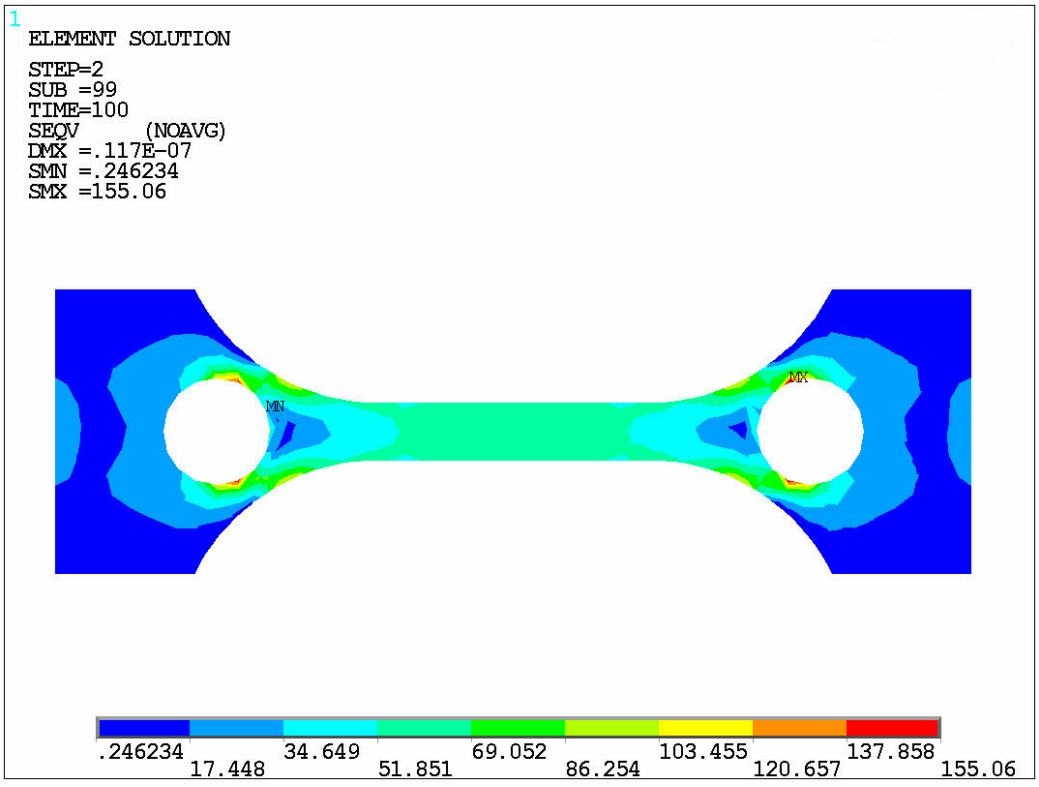

Fig 4.23: Creep stress redistribution: Equivalent stress at t=100

The stress redistribution in the critical area (i.e., at the hole stress concentration zone, gage length nominal stress section, neck stress concentration zone, head stress concentration zone, and the load-point applied stress area) due to creep are displayed in Figs. 4.24 and 4.25, respectively, for the initial and optimized designs of the specimen. As can be seen for both cases, there is a dramatic relaxation in the hole stress and relaxation also takes place in other areas.

It is also observed that a bigger equivalent stress is exactly located at the place where creep fracture may occur in the specimen. The analysis seems to suggest that creep failure follows a maximum strain criterion. Hence, if a design against early failure due to creep is to be implemented, then the stress redistribution and the total strain accumulation must be evaluated.

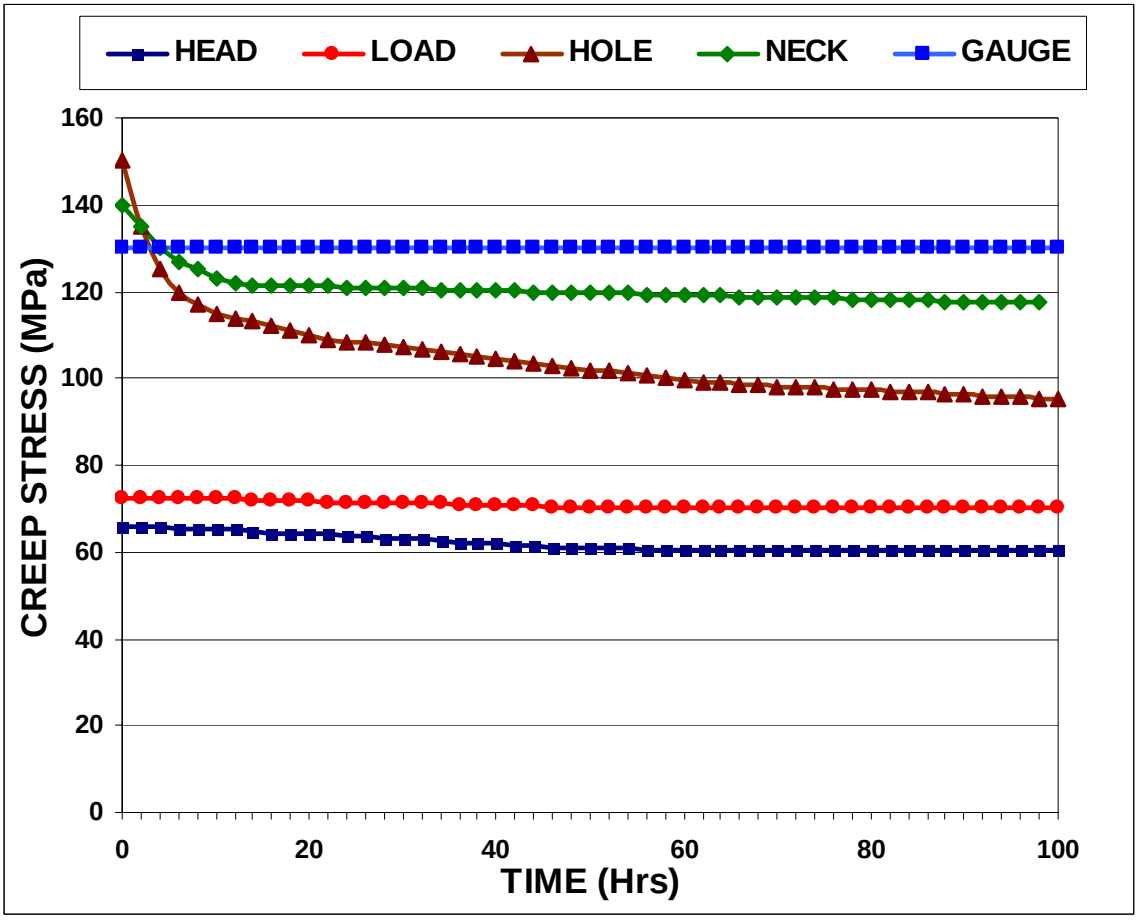

Fig. 4.24: Creep stresses experienced at various critical points as a function of time for initial specimen design

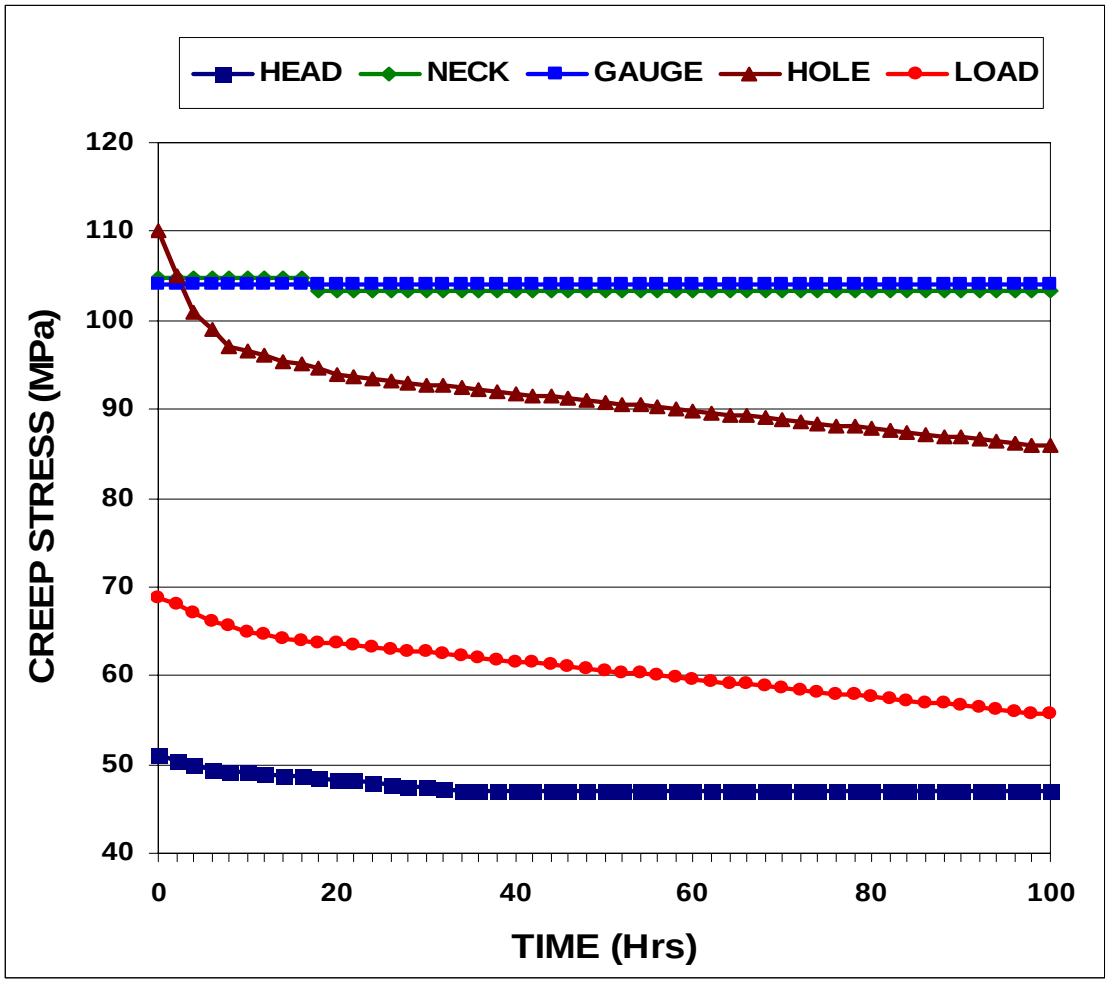

Fig. 4.25: Creep stresses experienced at various critical points as a function of time for final specimen design

The creep strain solutions in the critical areas are given in Fig. 4.26 and 4.27 for both cases. As can be seen, for the initial design, the accumulated strains at the hole edge are very high (Fig. 4.26). If the failure criterion of this material is such that failure will occur when the local strain exceeds the critical strain (or creep ductility), then the cracking from the pinhole will be observed at the location corresponding to this element. However, from Fig. 4.27 we see that the total creep strain at the hole edge has been reduced drastically. Thus, based on the critical strain failure criterion, the optimized specimen should not suffer premature failure during creep test.

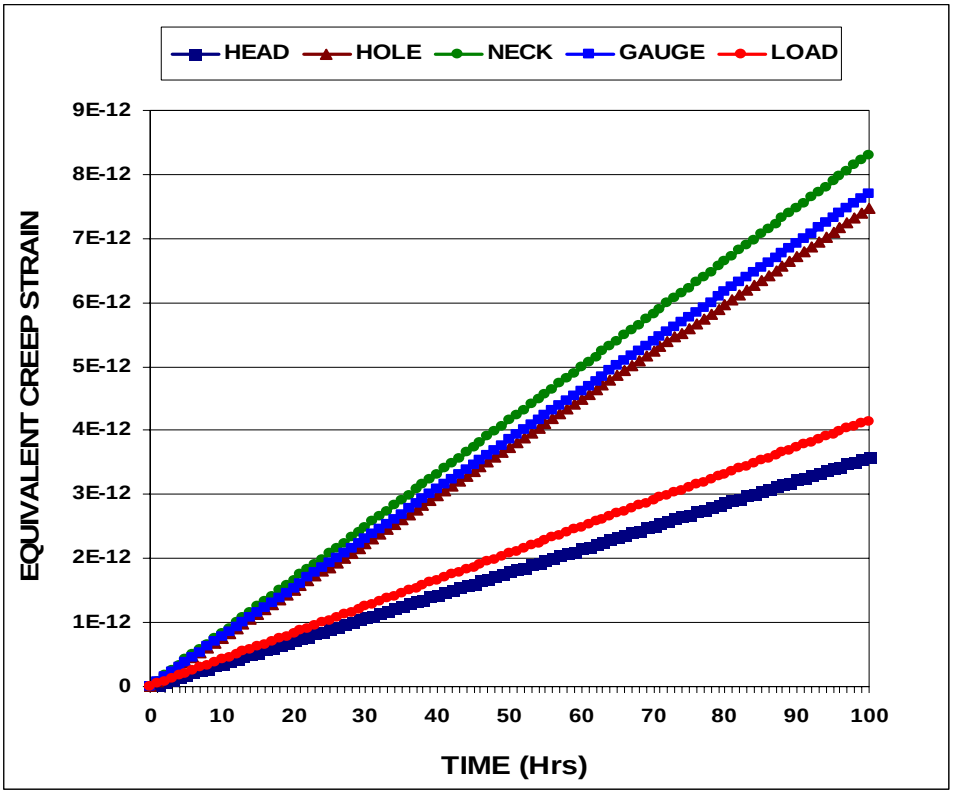

Fig. 4.26: Creep strains experienced at the corresponding locations for initial specimen design

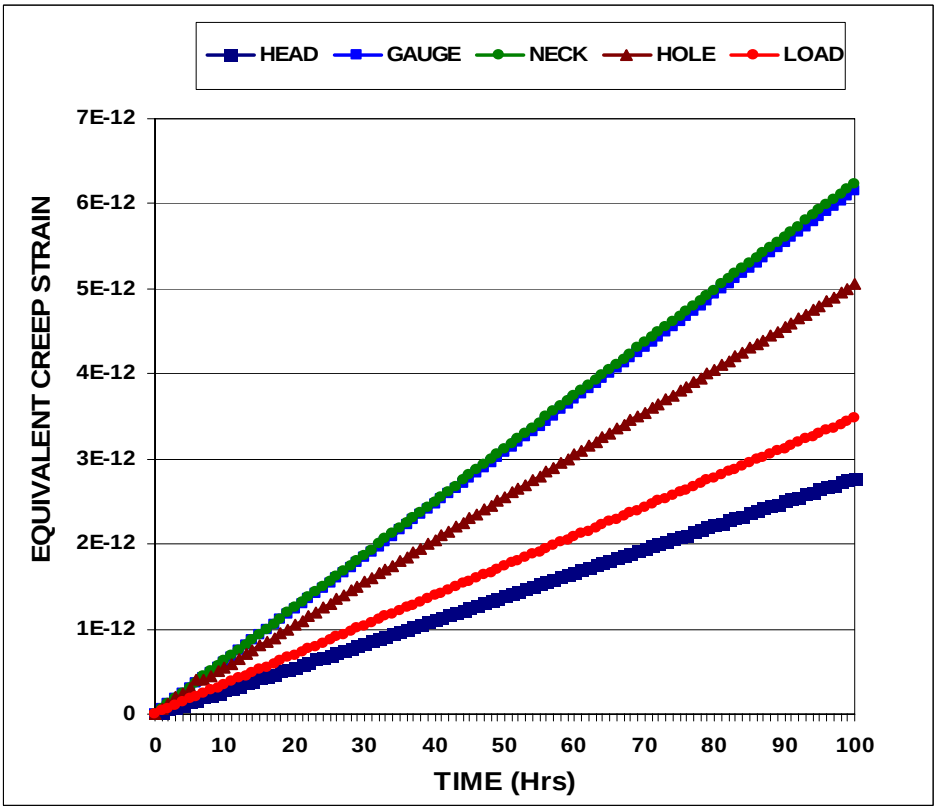

Fig. 4.27: Creep strains experienced at the corresponding locations for final specimen design

4.6 VALIDATION OF CREEP RESLUTS

The same program code was used for creep analysis of the initial and optimized specimen and the results were fairly matched. Figs. 4.28-4.32 show the compared results for creep stress at various critical zones for initial specimen.

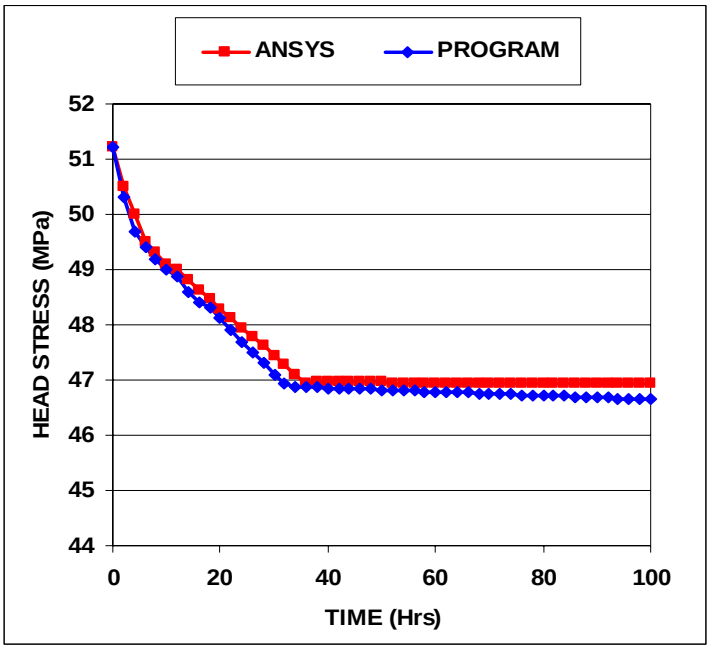

Fig. 4.28: Comparison of creep stress at head section (ANSYS vs Program: For Initial Specimen)

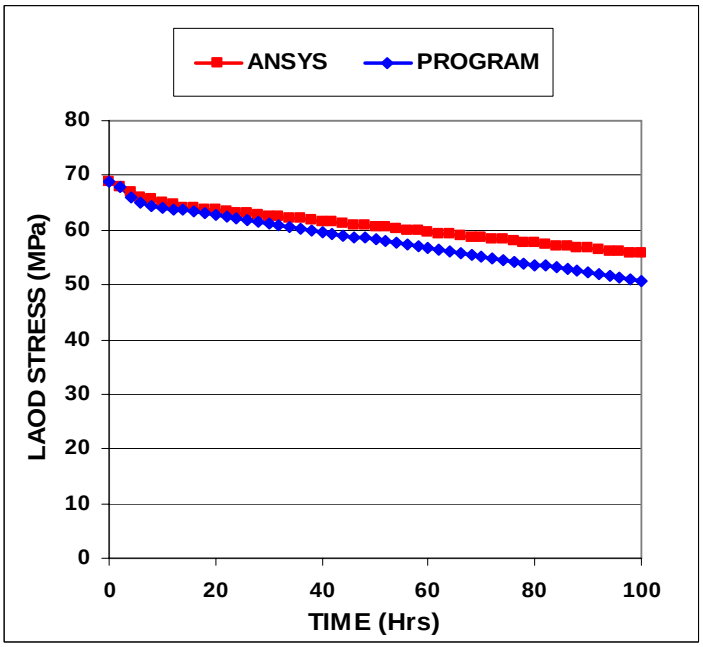

Fig. 4.29: Comparison of creep stress at load section (ANSYS vs Program: For Initial Specimen)

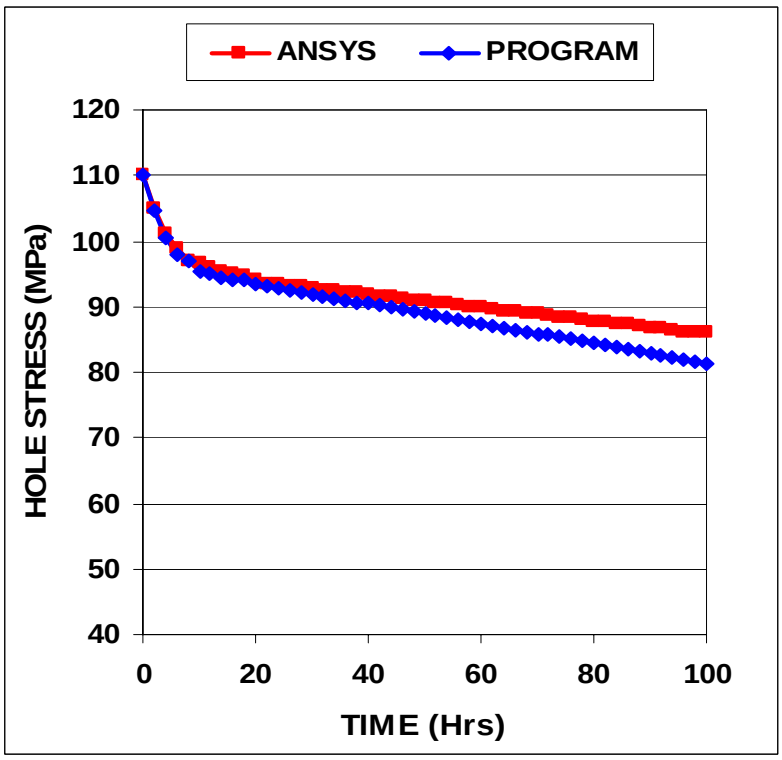

Fig. 4.30: Comparison of creep stress at hole section

(ANSYS vs Program: For Initial Specimen)

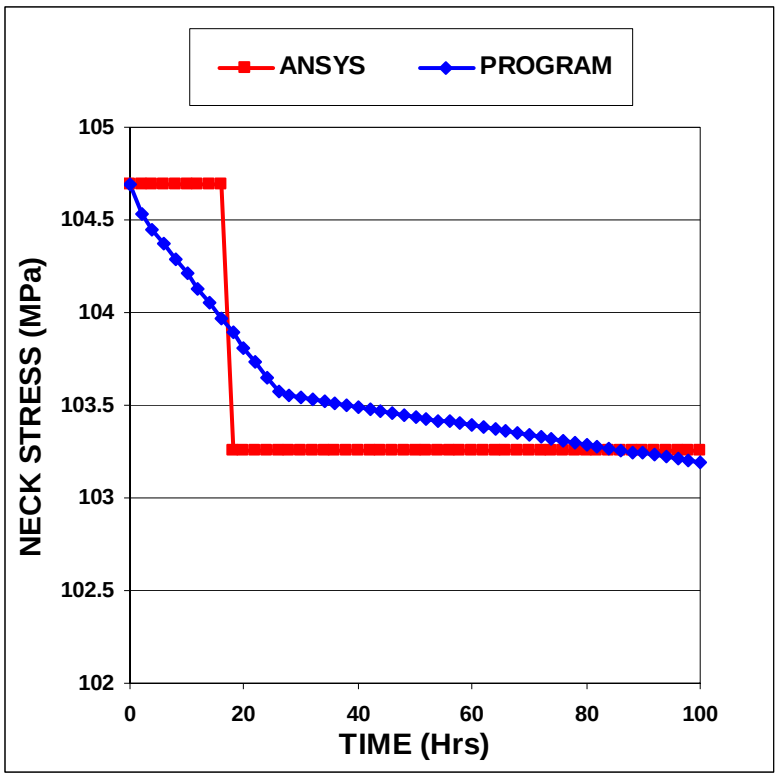

Fig. 4.31: Comparison of creep stress at neck section

(ANSYS vs Program: For Initial Specimen)

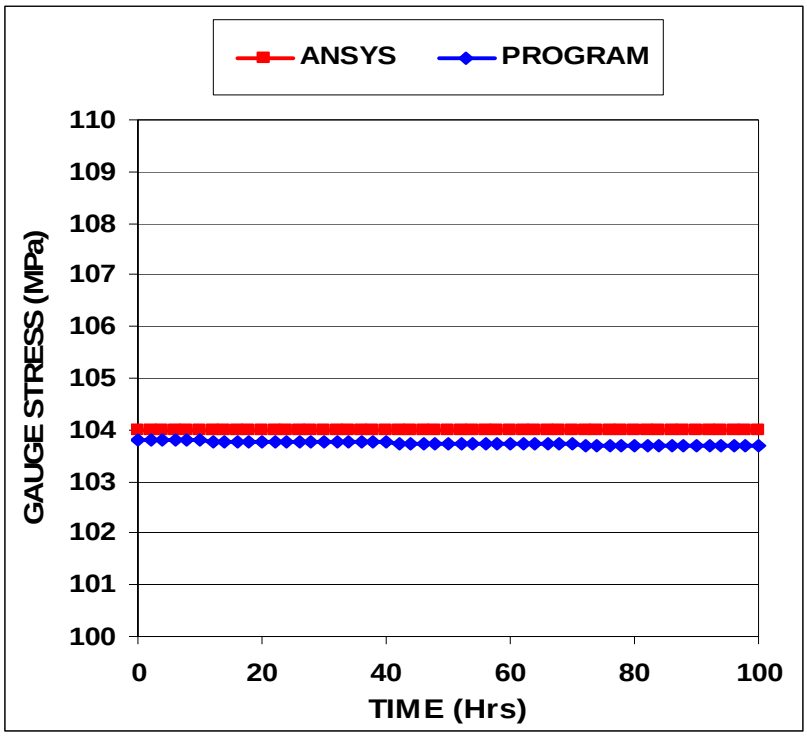

Fig. 4.32: Comparison of creep stress at gauge section

(ANSYS vs Program: For Initial Specimen)

Figs. 4.33-4.37 show the comparison of results for creep stress at various critical zones for optimized specimen.

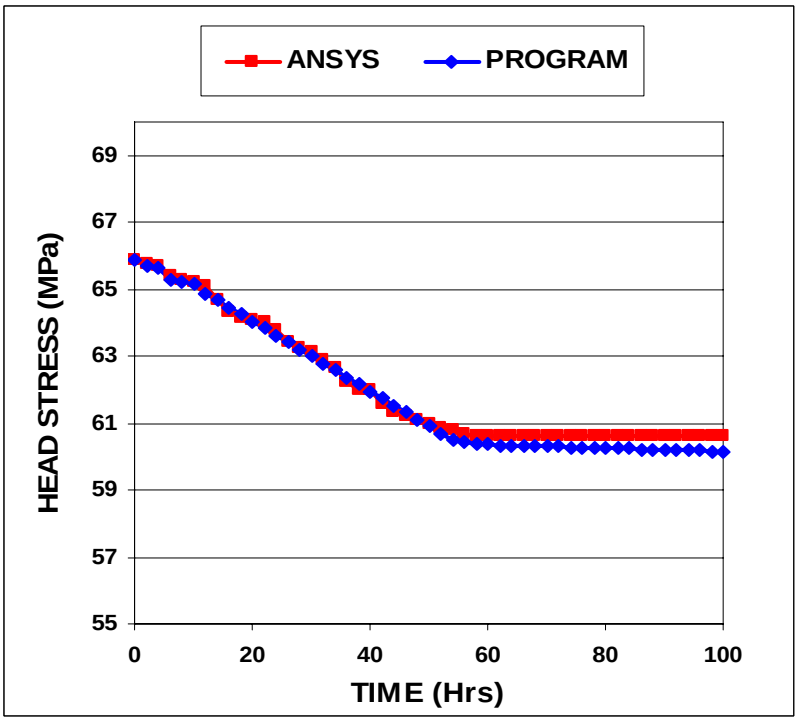

Fig. 4.33: Comparison of creep stress at head section

(ANSYS vs Program: For Optimized Specimen)

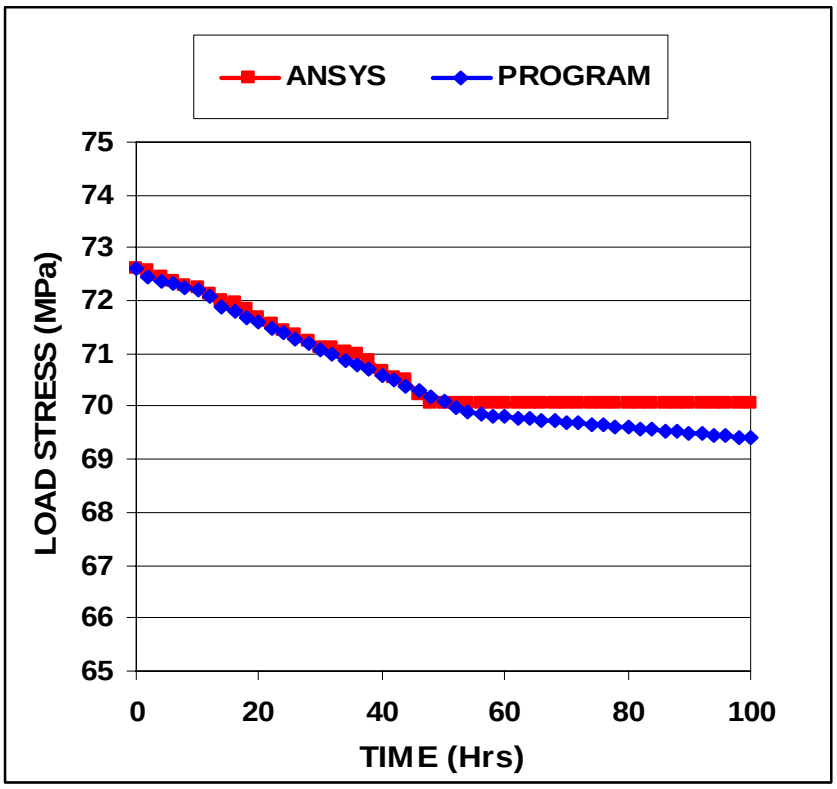

Fig. 4.34: Comparison of creep stress at load section

(ANSYS vs Program: For Optimized Specimen)

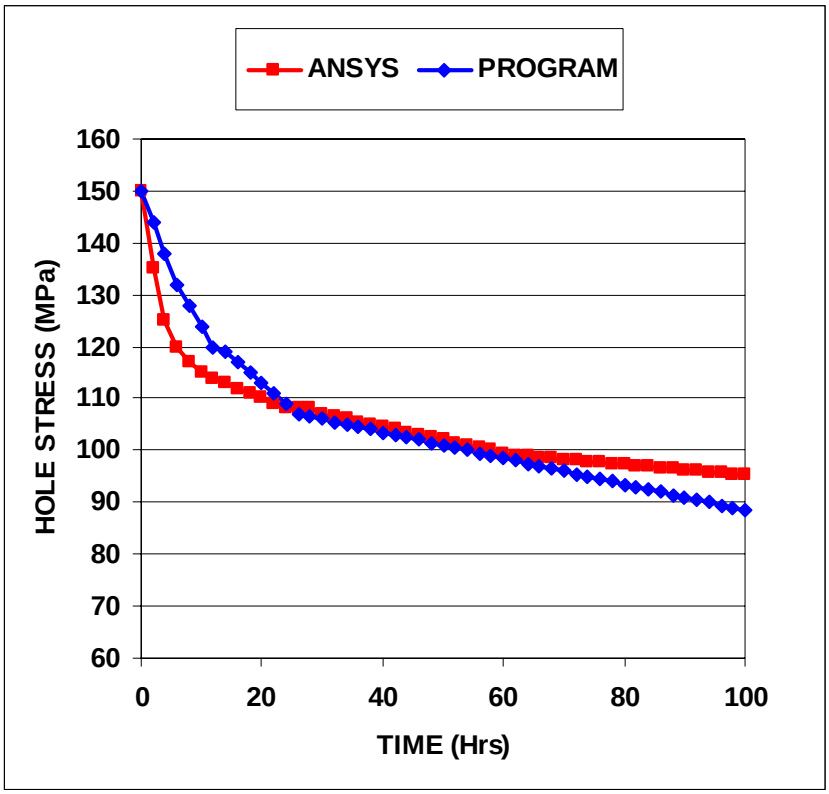

Fig. 4.35: Comparison of creep stress at hole section

(ANSYS vs Program: For Optimized Specimen

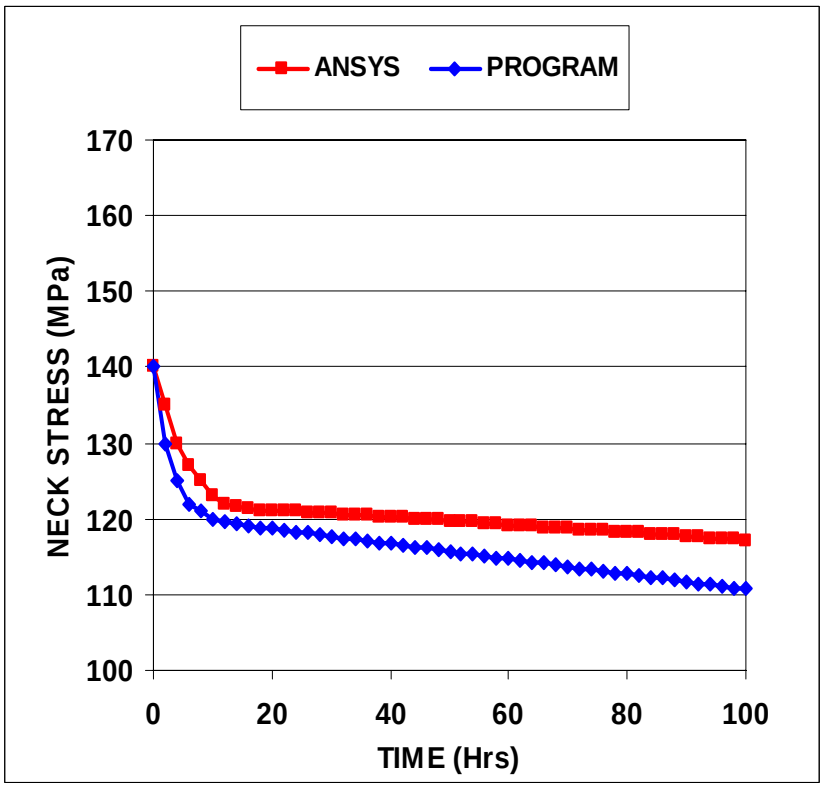

Fig. 4.36: Comparison of creep stress at neck section

(ANSYS vs Program: For Optimized Specimen)

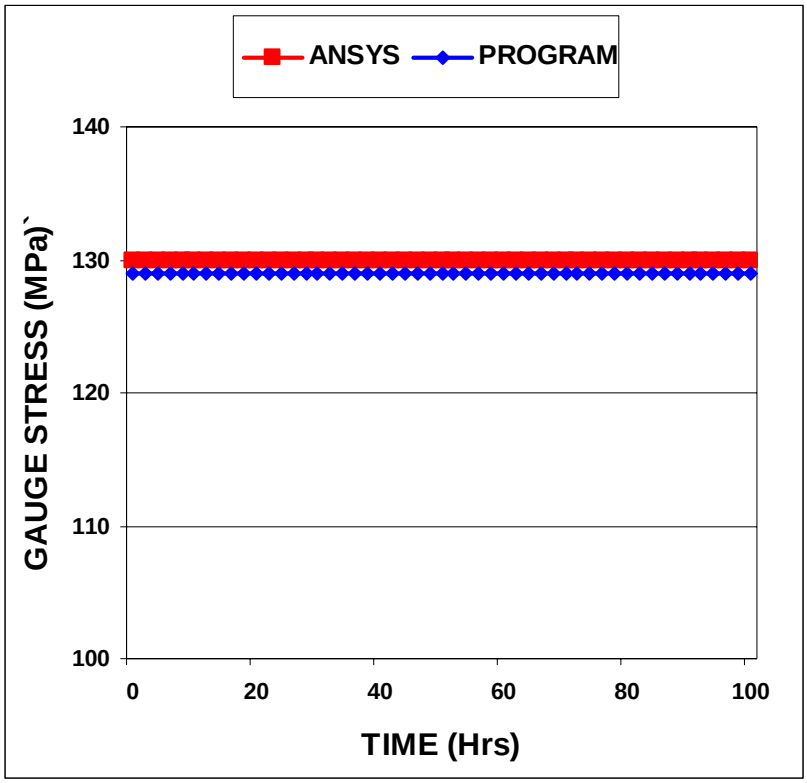

Fig. 4.37: Comparison of creep stress at gauge section

(ANSYS vs Program: For Optimized Specimen

Figs. 4.38-4.42 show the comparison of results for equivalent creep strain at various critical zones for initial specimen.

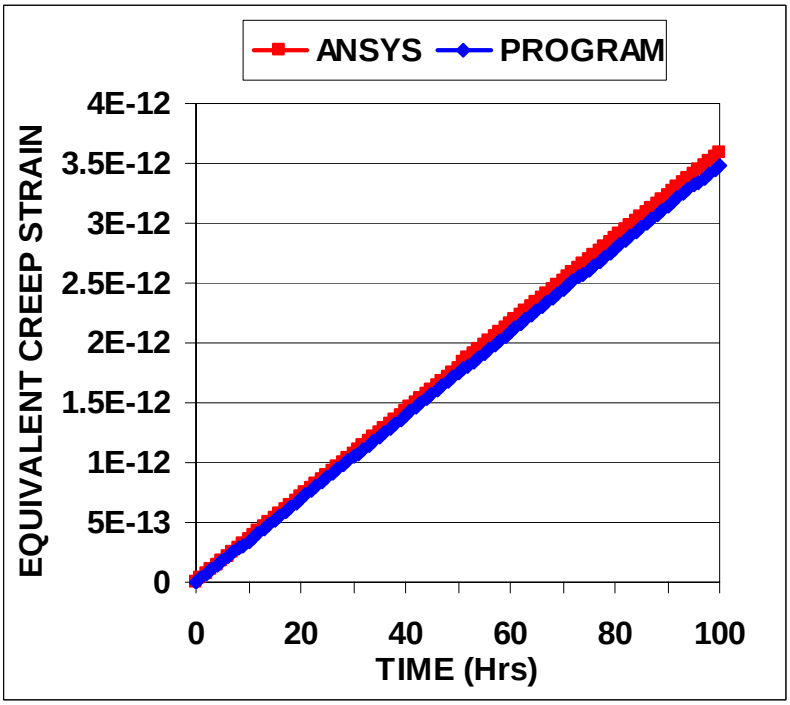

Fig. 4.38: Comparison of equivalent creep strain at head section (ANSYS vs Program: For Initial Specimen)

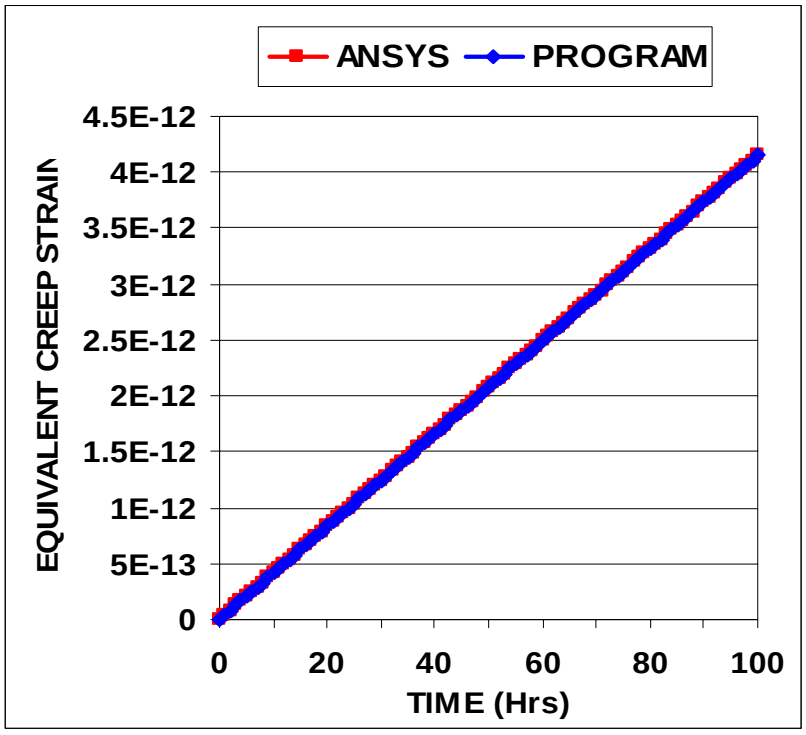

Fig. 4.39: Comparison of equivalent creep strain at load section (ANSYS vs Program: For Initial Specimen)

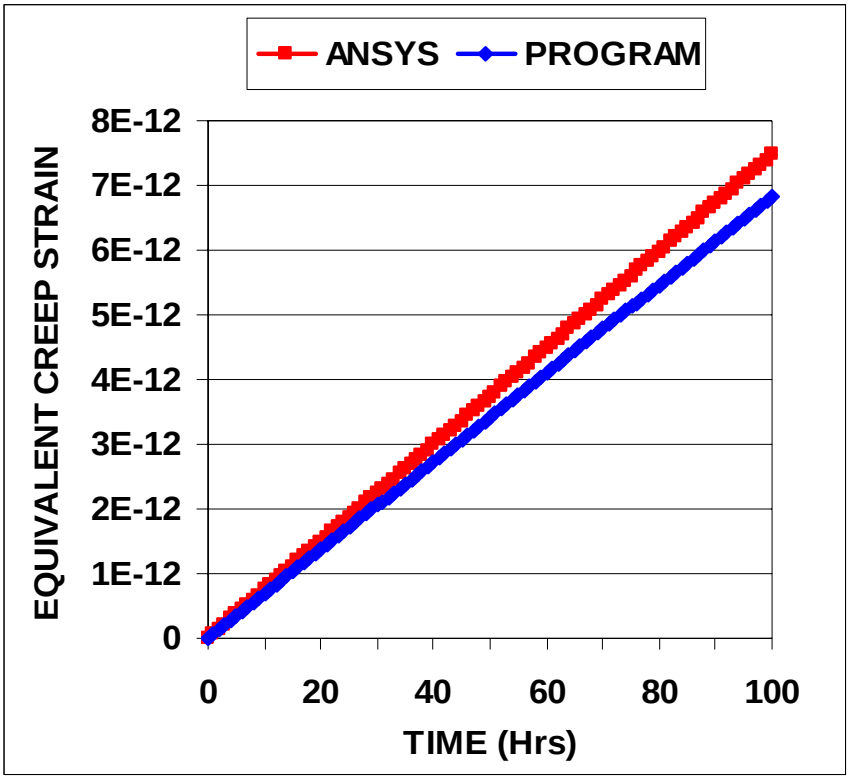

Fig. 4.40: Comparison of equivalent creep strain at hole section (ANSYS vs Program: For Initial Specimen)

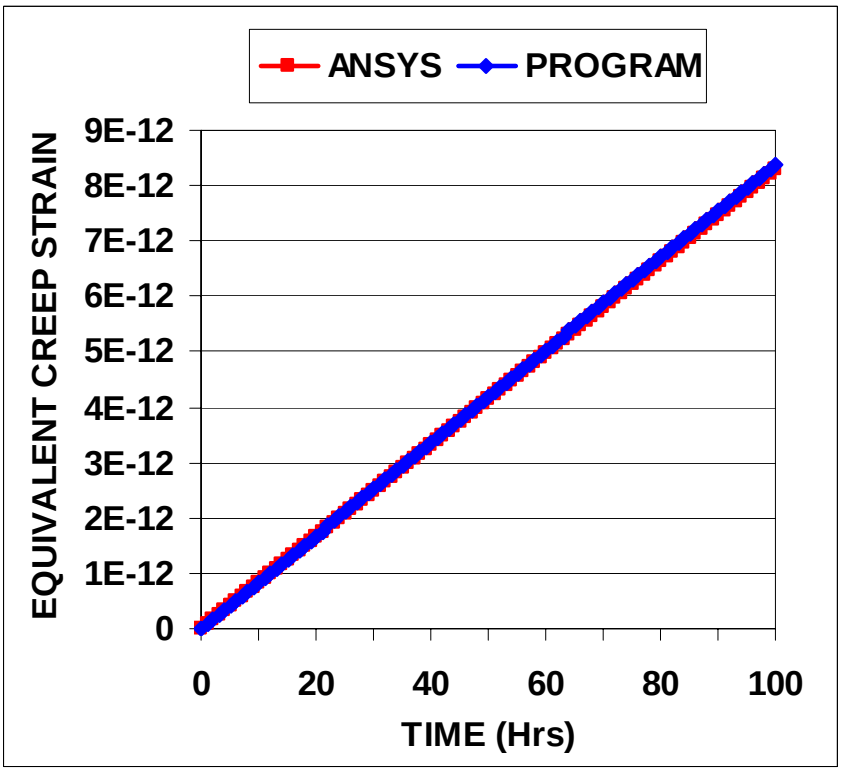

Fig. 4.41: Comparison of equivalent creep strain at neck section (ANSYS vs Program: For Initial Specimen)

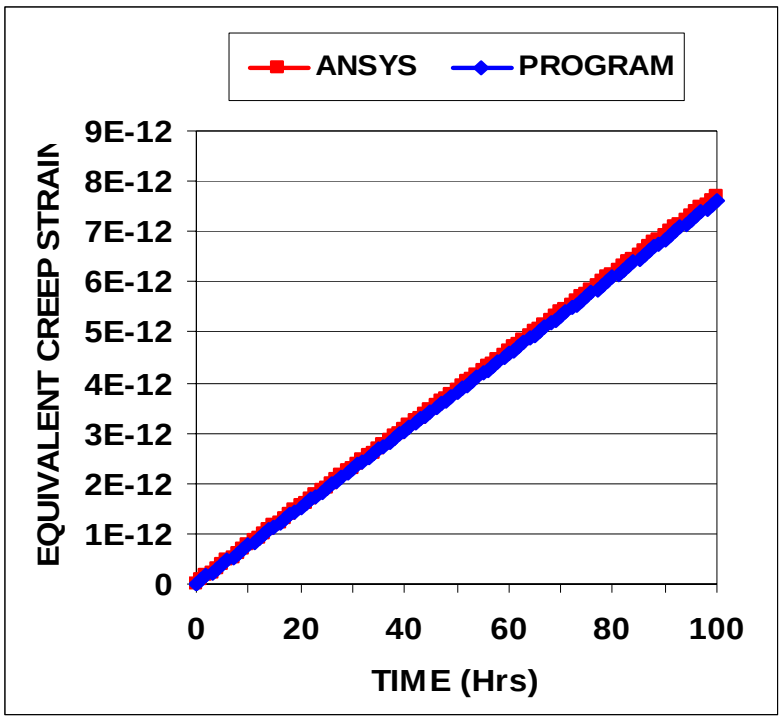

Fig. 4.42: Comparison of equivalent creep strain at gauge section

(ANSYS vs Program: For Initial Specimen)

Figs. 4.43-4.47 show the comparison of results for equivalent creep strain at various critical zones for optimized specimen.

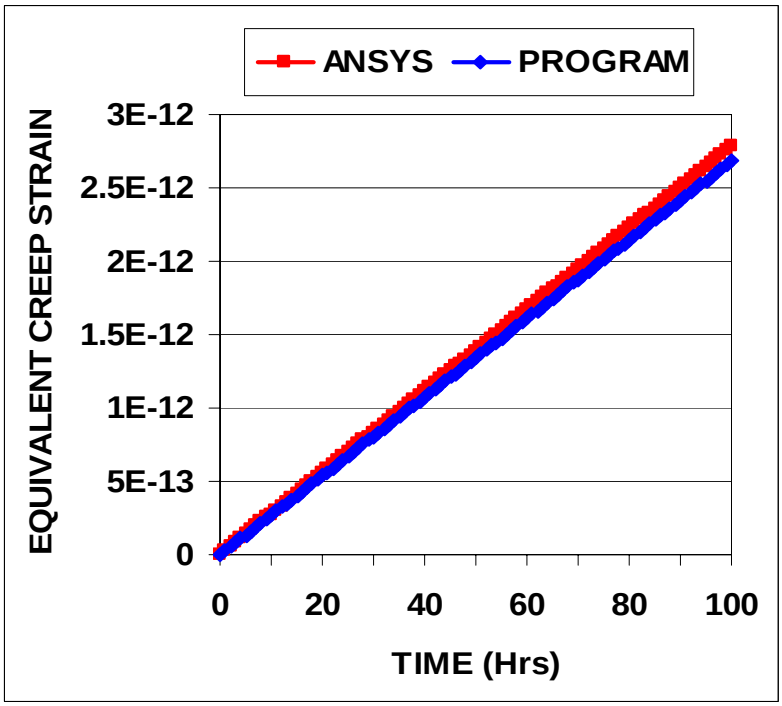

Fig. 4.43: Comparison of equivalent creep strain at head section

(ANSYS vs Program: For Optimized Specimen)

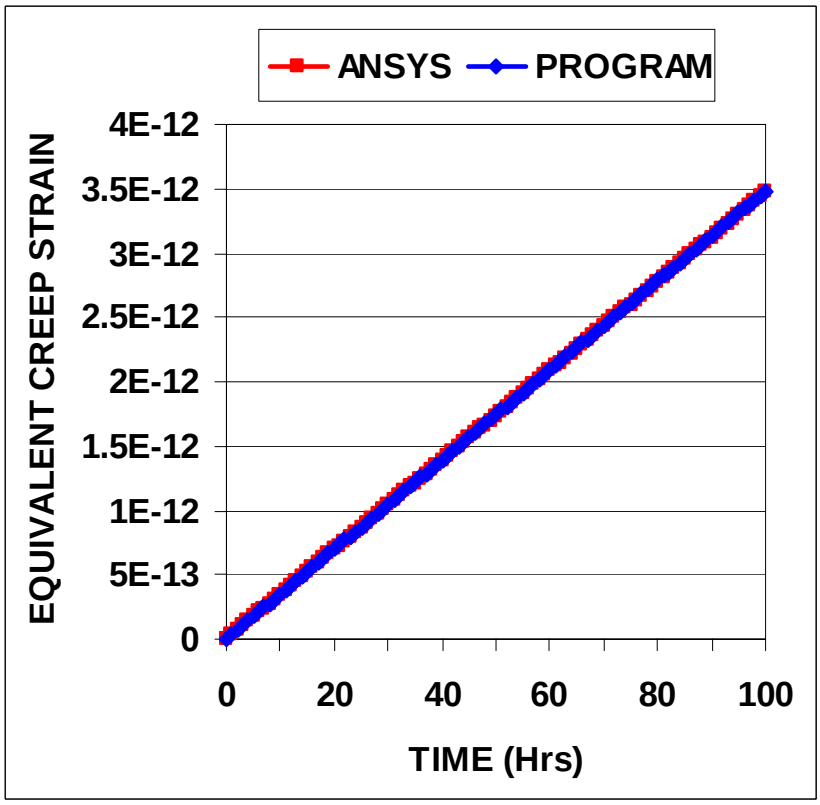

Fig. 4.44: Comparison of equivalent creep strain at load section

(ANSYS vs Program: For Optimized Specimen)

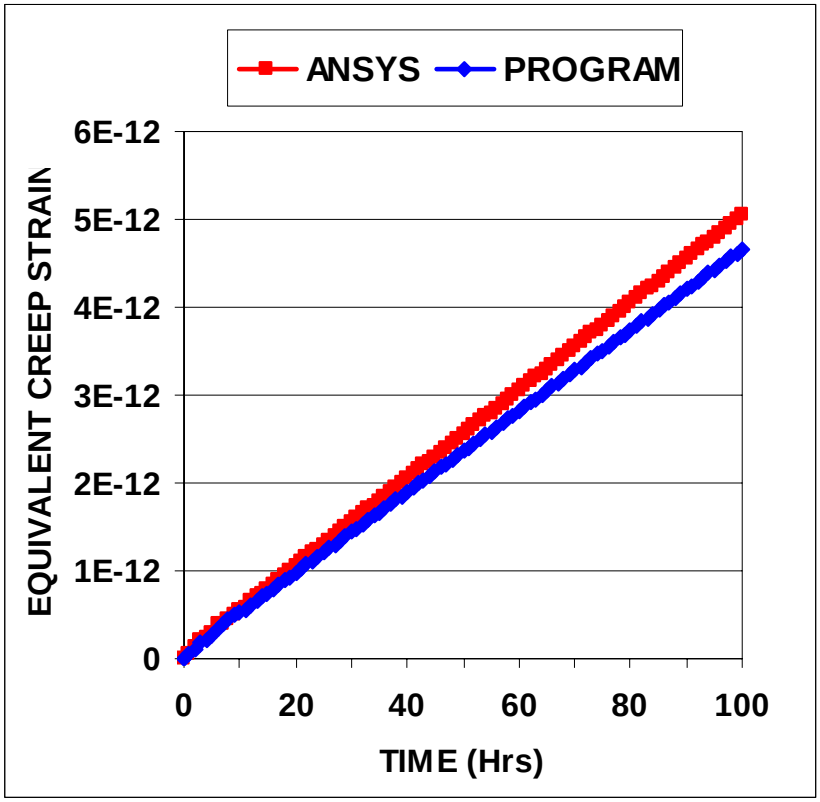

Fig. 4.45: Comparison of equivalent creep strain at hole section

(ANSYS vs Program: For Optimized Specimen)

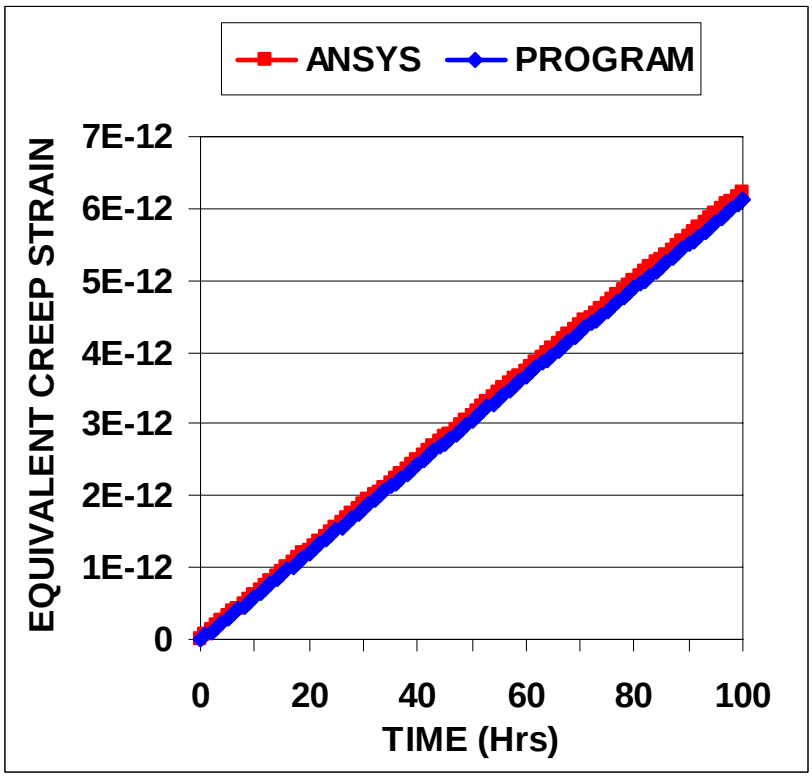

Fig. 4.46: Comparison of equivalent creep strain at neck section

(ANSYS vs Program: For Optimized Specimen)

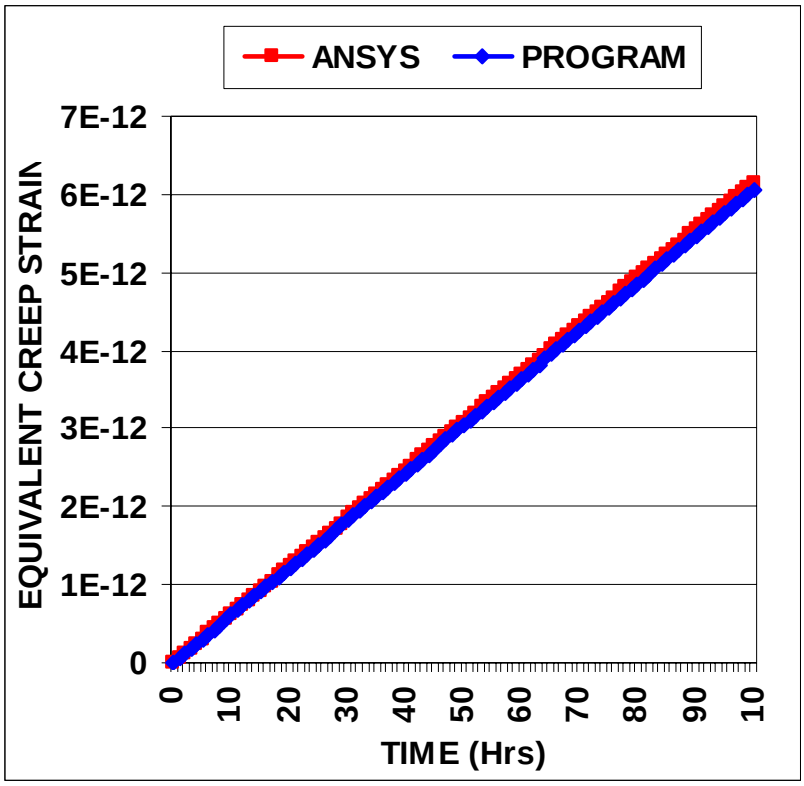

Fig. 4.47: Comparison of equivalent creep strain at gauge section

(ANSYS vs Program: For Optimized Specimen)

CHAPTER 5
CONCLUSION AND SCOPE FOR FUTURE WORK

5.1 CONCLUSION

Non-linear analysis of the ceramic tensile specimen is implemented using C++ which was validated with ANSYS. Then a complete time dependent creep analysis regarding the evolution of stress and strain as functions of time history is performed. The results indicated that the peak stresses and strains occurred at locations different from those predicted by elastic analysis. The creep analysis suggests that the creep failure follows a maximum strain criterion. Comparisons of creep stresses between initial and optimized specimens showed reduced severity, thereby lowering the probability of premature failure during creep test for the final design specimen.

5.2 SCOPE FOR FUTURE WORK

The present work can be extended to different ground. They are:

1) Higher order elements can be used to get more precise results.
2) Any other algorithm can be used to analyze creep in ceramics.

REFERENCES

1) D. F. Carroll and R. E. Tressler, "Accumulation of Creep Damage in a Siliconized Silicon Carbide", *J. Am. Ceram. Soc*., 71, 472–77 (1988).

2) S. M. Wiederhorn, D. E. Roberts, T.-J. Chuang, and L. Chuck, "Damage-Enhanced Creep in a Siliconized Silicon Carbide: Phenomenology", *J. Am. Ceram. Soc*., 71, 602–608 (1988).

3) Daniel F. Carroll and Richard E. Tressler, " Effect of Creep Damage on the Tensile Creep Behavior of a Siliconized Silicon Carbide", *J. Am. Ceram. Soc*., 72 (1), 49-53 (1989).

4) Daniel F. Carroll, Sheldon M. Wiederhorn and D. E. Roberts, "Technique for Tensile Creep Testing of Ceramics", *J. Am. Ceram. Soc*., 72 (9), 1610-1614 (1989).

5) Ching-Fong Chen and Tze-jer Chuang, "Improved Analysis for Flexural Creep with Application to Sialon Ceramics ",*J. Am. Ceram. Soc*., 73 (8), 2366-2373 (1990).

6) Ralph F. Krause Jr., "Observed and Theoretical Creep Rates for an Alumina Ceramic and a Silicon Nitride Ceramic in Flexure", *J. Am. Ceram. Soc*., 75 (5), 1307-1310 (1992).

7) Bernard J. Hockey and Sheldon M. Wiederhorn, "Effect of Microstructure on the Creep of Siliconized Silicon Carbide", *J. Am. Ceram. Soc*., 75 (7), 1822-1830 (1992).

8) John W. Holmes, "A Technique for Tensile Fatigue and Creep Testing of Fiber-Reinforced Ceramics", *Journal of Composite Materials*, 26 (6), 916-933 (1992).

9) C. J. Gasdaska, “Tensile Creep in an In Situ-Reinforced Silicon Nitride”, *J. Am. Ceram. Soc*., 77, 2408-18 (1994).

10) M. N. Menon, H. T. Fang, D. C. Wu, M. G. Jenkins, and M. K. Ferber, “Creep and Stress Rupture Behavior of an Advanced Silicon Nitride: II, Creep Rate Behavior”, *J. Am. Ceram. Soc*., 77, 1228-34 (1994).

11) Tatsuki Ohji and Yukihiko Yamauchi, “ Diffusional Crack Growth and Creep Rupture of Silicon Carbide Doped with Alumina”, *J. Am. Ceram. Soc*., 77 (3), 678-682 (1994).

12) Jow-Lian Ding, Kenneth C. Liu, Karren L. More and C. R. Brinkman, “Creep and Creep Rupture of an Advanced Silicon Nitride Ceramic”, *J. Am. Ceram. Soc*., 77 (4), 867-874 (1994).

13) Charles S. White, Ara M. Vartabedian b, Jon A. Wade b and Dennis M. Tracey b, “Notched tensile creep testing of ceramics”, *Materials Science and Engineering*, A203, 217-221 (1995).

14) William E. Luecke and Sheldon M. Wiederhorn, “Interlaboratory Verification of Silicon Nitride Tensile Creep Properties”, *J. Am. Ceram. Soc*., 80 (4), 831-38 (1997).

15) C.-W. Li and F. Reidinger, “Microstructure and Tensile Creep Mechanisms of an In Situ-Reinforced Silicon Nitride”, *Acta Mater*., 45 (1), 407-21 (1997).

16) Jacques Crampon and Richard Duclos, “Compressive Creep and Creep Failure of $8Y_2O_3/3Al_2O_3$-Doped Hot-Pressed Silicon Nitride”, *J. Am. Ceram. Soc*., 80 (1), 85-91 (1997).

17) R. F. Krause Jr., W. E. Luecke, S. M. Wiederhorn, J. D. French, and B. J. Hockey, “Tensile Creep and Rupture of Silicon Nitride”, *J. Am. Ceram. Soc*., 82 (5), 1233-41 (1999).

18) Sheldon M. Wiederhorn and William E. Luecke, “Comparison of Tensile and Compresive Creep Behavior in Silicon Nitride”, *J. Am. Ceram. Soc*., 83 (8), 2017-22 (2000).

19) Ralph F. Krause Jr. and Sheldon M. Wiederhorn, “Tensile Creep Behavior of a Gas-Pressure-Sintered Silicon Nitride Containing Silicon Carbide”, *J. Am. Ceram. Soc*., 84 (10), 2394-400 (2001).

20) Tatsuki Ohji, “High-Temperature Reliability of Advanced Ceramics”, National Industrial Research Institute of Nagoya, *ASME*, 123 (2001).

21) William E. Luecke, “Results of an International Round-Robin for Tensile Creep Rupture of Silicon Nitride”, *Journal J. Am. Ceram. Soc*., 85 (2), 408-14 (2002).

BIBLIOGRAPHY

1) G. A. Greenbaum and M. F. Rubinstein, "Creep Analysis of Axisymmetric Bodies Using Finite Elements", *Nucl. Eng. Design*, 7, 379 (1968).

2) W. D. Kingery, H. K. Bowen and D. R. Uhlmann, Introduction to Ceramics (Second Edition), John Wiley & Sons, 1976.

3) O.C.Zienkiewicz, The Finite Element Method, Tata McGraw-Hill Publication, London, 1979.

4) Mel M. Scwartz, Engineering Applications of Ceramic Materials (Source Book, A Collection of Outstanding Articles from Technical Literature), American Society for Metals, Ohio, 1985.

5) T. J. Chuang, "Estimation of Power-Law Creep Parameters from Bend Test Data", *J. Mat. Sci*., 21 (2), 165-175 (1986).

6) K. C. Liu, H. Pih and D. W. Voorhes, "Uniaxial Tensile Strain Measurement for Ceramic Testing at Elevated Temperatures: Requirements, Problems and Solutions", *Int. J. High Tech. Ceram*., 4, 161-171 (1988).

7) Shinroku, Advanced Ceramics, Oxford Science Publications and Ohmsha Ltd, 1988.

8) S. M. Wiederhorn, D. E. Roberts, T. J. Chuang and L. Chuck, "Damage-enhanced Creep in Siliconized Silicon Carbide: Phenomenology", *J. Am. Ceram. Soc*., 71 (3), 602-608 (1988).

9) D. F. Carroll, S. M. Wiederhorn and D. E. Roberts, "Technique for Tensile Creep Testing of Ceramics", *J. Am. Ceram. Soc*., 72, 1610-1614 (1989).

10) M. K. Ferber, M. G. Jerkins and V. J. Tennery, "Comparison of Tension, Compression and Flexural Creep for Alumina and Silicon Nitride", *Ceram. Eng. Sci. Proc.*, 11 (7), 1028-1045 (1990).

11) F. J. Wu, "Design Optimization of Norton's Ceramic Creep Dog-Bone Specimen", TM 91-29, *Saint-Gobain/Norton Industrial Ceramic Corp*., Northboro, MA, (1991).

12) S. M. Wiederhorn, R. J. Gettings, D. E. Roberts, C. Ostertag. and J. J. Petrovic, "Tensile Creep of Silicide Composites", *Mat. Sci. Eng*., A155, 209-215 (1992).

13) R. F. Krause, "Observed and Theoretical Creep Rates for an Alumina Ceramic and Silicon Nitride Ceramic in Flexure", *J. Am. Ceram. Soc*., 75 (5), 1307-1310 (1992).

14) T. Ohji and Y. Yamauchi, "Long-Term Tensile Creep Testing for Advanced Ceramics", *J. Am. Ceram. Soc*., 75 (8), 2304-2307 (1992).

15) J. N. Reddy, Finite Element Method, McGraw-Hill International Editions, London, 1993.

16) R. B. Thayer and J.-M. Yang, "Creep Behavior of SiC Fiber-Reinforced Hot-Pressed Si3N4 Composites", *Mat. Sci. Eng*., A160, 169-179 (1993).

17) R. B. Thayer and J. M. Yang, "Analysis of Flexural Creep for an SiC Fiber-Reinforced Si3N4 Composite", *J. Mat. Sci*., 29, 693-699 (1994).

18) R. Tirupathi Chandrupatla and D. Ashok Belegundu, *Introduction* to Finite Elements in Engineering, Prentice Hall of India Pvt Ltd, New Delhi, 1997.

19) R. Tirupathi Chandrupatla and D. Ashok Belegundu, Introduction to Finite Elements in Engineering, Printice Hall of India Pvt Ltd, New Delhi, 1997.

20) ROBERT LAFORE, Object-Oriented Programming in Turbo C^{++}, Galgotia Publication Pvt. Ltd. New Delhi, 2000.

21) David V. Hutton, Fundamentals of Finite Element Analysis, McGraw-Hill International Edition, 2004.

22) J. N. Reddy, An Introduction to Nonlinear Finite Element Analysis, Oxford University Press, London, 2004.